Eur. J. Mineral., 36, 247–266, 2024
https://doi.org/10.5194/ejm-36-247-2024

European Journal of Mineralogy
Open Access

Crystal chemistry and molar volume of potassic-chloro-hastingsite

Jared P. Matteucci[1], **David M. Jenkins**[1], **and M. Darby Dyar**[2]

[1]Department of Earth Sciences, Binghamton University, Binghamton, NY 13902-6000, USA
[2]Department of Astronomy, Mount Holyoke College, South Hadley, MA 01075-1429, USA

Correspondence: Jared P. Matteucci (jmatteu1@binghamton.edu)

Received: 3 October 2023 – Revised: 20 December 2023 – Accepted: 7 January 2024 – Published: 1 March 2024

Abstract. Several geological processes such as crustal and mantle metasomatism, high-grade metamorphism, and the formation of ore deposits involve the exchange of halogens, especially chlorine, between silicate minerals and fluids. It is well established that the presence of octahedral iron is vital to the process of Cl incorporation into amphiboles. However, other compositional controls on Cl incorporation, such as the effect of ^{T}Al, ^{A}Na, ^{A}K, and A-site occupancy are not as well constrained. This study reports on the compositional and structural relationships amongst a suite of 25 synthetic calcium amphiboles with a diverse range of Cl contents (0–1.68 atoms per formula unit (apfu)). Most amphiboles were synthesized along the potassic-hastingsite–potassic-chloro-hastingsite join ($KCa_2(Fe_4Fe^{3+})(Al_2Si_6)O_{22}(OH,Cl)_2$). Additional work involved substitution of Na for K, variable Al content, and substitution of Mg for Fe^{2+} in the bulk composition to explore these compositional effects on Cl incorporation. The relationship between pressure and the Cl content of amphiboles was also explored over the pressure range 0.3–2.0 GPa. Otherwise, synthesis conditions were 700 °C and 0.3 GPa with fO_2 near Ni–NiO. Iron (II) chloride was used as the source of Cl. Some experiments used variably concentrated $FeCl_2$ brines (0–100 molal), while others were nominally anhydrous, containing only the water absorbed by the hygroscopic $FeCl_2$. All amphiboles were characterized by Rietveld refinements of powder X-ray diffraction patterns, electron microprobe analysis, and Mössbauer spectroscopy, the latter to determine Fe^{3+} fraction. This study finds a positive relationship between pressure and the Cl content of the amphibole. Both Fe^{2+} and Fe^{3+} are positively correlated with Cl among amphiboles with variable Fe#, but the correlation is poor to nonexistent for Mg-free amphiboles. Results indicate that the substitution of $^{C}Fe^{2+,3+}$ for ^{C}Mg and $^{C}Fe^{2+,3+}$ for ^{C}Al facilitate Cl incorporation, with the former having a larger effect. The A-site occupancy is positively correlated with Cl in all amphiboles except those synthesized in dilute $FeCl_2$ brines ($\leq 6\,m$), which are negatively correlated. No correlation is observed between the Cl content of the amphibole and either the species of A cation (K vs. Na) or ^{T}Al. The composition vs. unit cell parameter data were analyzed using multivariate linear regression to better understand the process of Cl incorporation and to predict the molar volume of endmember chloro-amphiboles. The regression indicates an expansion of 0.181 Å (0.99 %) and 0.048 Å (0.90 %) along the b and c edges respectively, a reduction in β by 0.76° (0.72 %), and a contraction of 0.060 Å (0.59 %) along a when fully substituting Cl for OH in potassic-hastingsite. The multivariate linear regression equations allow the prediction of molar volumes for select endmember chloro-amphiboles, such as potassic-chloro-hastingsite $= 964.63 \pm 1.29$ Å^3 or 290.5 ± 0.4 cm^3 mol^{-1}.

Published by Copernicus Publications on behalf of the European mineralogical societies DMG, SEM, SIMP & SFMC.

1 Introduction

Chorine is an important component of natural aqueous fluids, playing an important role in many geological processes including high-grade metamorphism (Newton et al., 1998), mantle metasomatism (Frezzotti et al., 2011; Selverstone and Sharp, 2011), crustal and shear-zone metasomatism (Kusebauch et al., 2015), seawater–ocean crust interaction (Barnes and Cisneros, 2012; Kendrick et al., 2015), and the formation of ore deposits (Yardley and Bodnar, 2014). In the absence of primary fluid inclusions, the halogen activity of aqueous fluids can be determined using the compositions of equilibrium volatile-bearing (OH^-, Cl^-, F^-) phases, such as amphiboles or sheet silicates. However, this is not a simple task because several variables affect the partitioning of halogens between silicate minerals and aqueous fluids, including the halogen activity of the fluid, composition of the mineral, and pressure–temperature conditions. This study focuses specifically on examining the various compositional controls on Cl incorporation into the calcium amphiboles potassic-chloro-hastingsite and chloro-hastingsite.

Current knowledge of the crystal chemical controls on Cl incorporation into amphiboles is incomplete, with some aspects that are better understood than others. For example, it has been well established that Fe# ($Fe^{2+}/(Fe^{2+}+Mg)$) plays a crucial role in controlling which monovalent anion is preferred on the O(3) site. This tendency has been termed Mg–Cl/Fe–F avoidance and is ubiquitous among reports of natural and synthetic amphiboles and sheet silicates (Ekström, 1972; Volfinger et al., 1985; Castelli, 1988; Enami et al., 1992; Kullerud, 1996; Léger et al., 1996; McCormick and McDonald, 1999; Xiao et al., 2005; Liu et al., 2009; Kendrick et al., 2015; Henry and Daigle, 2018). No examples are known that show the opposite. Other compositional constraints on Cl incorporation are, however, not so well understood, which include ^{A}K replacing ^{A}Na, ^{A}X replacing $^A\square$ (X = Na or K, $\square$ = vacancy), and ^{T}Al replacing ^{T}Si. At the *A* site, naturally occurring amphiboles consistently show a positive correlation between the *A*-site occupancy and Cl (e.g., Morrison, 1991; Enami et al., 1992; Sautter et al., 2006; Xiao et al., 2005; Yu et al., 2017). However, there are conflicting data regarding the influence of the specific *A*-site cation. Matteucci et al. (2024) review the trends between the *A*-site cation and Cl content of natural amphiboles, finding that there are essentially two tendencies: (1) both ^{A}K and ^{A}Na are positively correlated with Cl, and (2) ^{A}Na and Cl are negatively correlated while ^{A}K and Cl are positively correlated. These observations have been historically interpreted to indicate that ^{A}K for ^{A}Na substitution asserts some degree of control on Cl incorporation into amphibole. However, a positive correlation is not always reported between ^{A}K and Cl, most notably in Liu et al. (2009). Finally, positive correlations are often reported between ^{T}Al and Cl (Kullerud, 1996; Léger et al., 1996; McCormick and McDonald, 1999; Xiao et al., 2005; Henry and Daigle, 2018), suggesting a preference for Al over Si on the *T* sites in Cl-rich amphiboles. It is possible that correlations between *A*-site occupancy and Cl as well as ^{T}Al and Cl are due to the edenite substitution ($^A\mathrm{X} + {}^T\mathrm{Al} = {}^A\square + {}^T\mathrm{Si}$), which would cause both cations to have positive correlations with Cl. Thus, use of compositional trends in natural amphiboles is complicated by not only the large number of compositional variables (^{A}Na, ^{A}K, ^{T}Al, and Fe#) of the host amphibole structure, but also the effect of variable anion concentration in the ambient brine as well as the largely unknown influence of variable temperature (*T*), pressure (*P*), and oxygen fugacity. A more reliable approach to understanding the process of Cl incorporation is to take an experimental approach, where it is possible to hold certain key variables constant.

There have been few experimental studies of chloro-amphiboles, especially those that explore the crystal chemical controls on Cl incorporation. The first studies exploring the process of Cl incorporation into silicate minerals were of micas. Volfinger et al. (1985) have shown how the octahedral cation present in biotite affects its propensity to incorporate Cl, considering Mg, Ni, Co, and Fe. The study found that the ability of biotite to incorporate Cl is dependent on the size of the octahedral cation, with larger cations supporting larger amounts of Cl. This is attributed to the degree of distortion of the tetrahedral rings, which was smallest when the large cation Fe^{2+} was present at the octahedral sites, allowing for more space in the cavity to be occupied by Cl. For the same reason, the paper hypothesizes that small cations at the tetrahedral sites (Si at 0.26 Å vs. Al at 0.39 Å radii) should encourage Cl uptake.

Oberti et al. (1993) determined a mechanism for Cl incorporation into amphiboles based on both structure constraints and bond strength considerations. The study used single-crystal X-ray diffraction to refine the structures of three hastingsitic amphiboles, with Cl contents ranging from 0 to 0.98 atoms per formula unit (apfu). They found that Fe^{2+} orders strongly into the *M*(1) and *M*(3) sites, which directly bond with the O(3) anion, suggesting a preference for Fe–Cl bonds over Mg–Cl bonds. Furthermore, the bonding interaction between the *A* and O(3) site is enhanced when K is the A cation. The paper argues that because K preferentially orders into the *Am* site, which is the closest position to the O(3) site that the A cation can occupy, a stronger bond is present between ^{A}K and Cl than ^{A}Na and Cl. This is hypothesized to contribute to positive correlations between K and Cl in natural amphiboles. The paper also maintains that lengthening of the tetrahedral chain must be required for it to remain linked to the expanding octahedral strip as $^C Fe^{2+}$ replaces $^C Mg^{2+}$ during Cl incorporation. This can be accomplished either by straightening of the tetrahedral chain or enlargement of the tetrahedral sites by the substitution of Al for Si. The paper asserts that the tetrahedral chain cannot straighten to the degree required to provide sufficient lengthening for endmember chloro-hastingsite ($(Na,K)Ca_2(Fe_4Fe^{3+})(Al_2Si_6)O_{22}Cl_2$). Therefore, some ex-

pansion of the tetrahedral sites by Al incorporation is necessary.

Mueller et al. (2017) explored the effects of Fe^{2+}–Mg substitution on Cl incorporation into hastingsitic amphiboles. The study found a generally positive correlation between Fe# and the Cl content of the amphibole as well as a negative correlation between the Fe^{3+} fraction and Cl. Surprisingly, their most Fe-rich amphibole (Fe# = 1.0) did not contain the highest amount of Cl; rather, it was the amphibole with Fe# 0.7, which had a Cl content of 0.42 apfu.

Jenkins (2019) presented results on synthesized amphiboles with bulk compositions equivalent to chloro-hastingsite, potassic-chloro-hastingsite, and chloro-ferropargasite. One series of experiments includes hastingsitic amphiboles with variable K/(Na + K) fractions (= K#) ranging from 0–1 under nominally anhydrous conditions, meaning that water was not purposely added to the system during synthesis. These amphiboles had a positive correlation between K and Cl, similar to what is observed in many natural amphiboles. Furthermore, the paper calculated the brine Cl concentration present in each charge at the end of the experiments by puncturing the capsules and heating them to 110 °C to drive off any volatiles, which were assumed to be water. Though each charge was initially virtually anhydrous, an evolved brine becomes established at some point during treatment. The source of water may be moisture absorbed by the hygroscopic $FeCl_2$ reagent or diffusion of oxygen-buffering hydrogen into the capsule, which then reacts with any oxygen present (free or in the reagent Fe_2O_3) to form water. A weak positive correlation between the brine Cl concentration and the Cl content of the amphibole ($r = 0.53$) was observed, while a better correlation between K and Cl ($r = 0.84$) was found. Jenkins (2019) also observed no correlation between ^{T}Al and Cl (though the study did not specifically explore this), no correlation between temperature and Cl (temperatures ranged from 700 to 900 °C), and no correlation between pressure and Cl (pressures ranged from 0.2–0.45 GPa).

The relationship between the A cation and Cl content of hastingsitic amphiboles (Fe# = 1.0) in the presence of variably concentrated $FeCl_2$ brines is explored in Matteucci et al. (2024). The study synthesized a series of amphiboles with constant brine $FeCl_2$ concentration for which the K# of the bulk composition was varied from 0 to 1 in 0.25 increments. This was repeated, exploring a total of five different $FeCl_2$ brine concentrations, ranging from 1–100 molal (m). The paper found no correlation between the Cl content of the amphibole and the K#; the Cl content of the amphibole was solely constrained by the brine $FeCl_2$ concentration. In contrast to the study of Jenkins (2019), Matteucci et al. (2024) used the initial brine Cl concentration, or the brine Cl concentration before treatment, which was calculated from the amount of water added to each charge, including any water contained within the $FeCl_2 \cdot nH_2O$ reagent. The paper also calculated the final brine Cl concentration, as in Jenkins (2019), and found that method to be less reliable. It tended to overestimate the Cl concentration in the brine because of the presence of bound water within $FeCl_2 \cdot nH_2O$, which is typically present at the end of experiments that used $FeCl_2$ as a reagent. This casts doubt on the actual brine concentrations determined for the nominally anhydrous syntheses done by Jenkins (2019), suggesting it is possible that the positive correlation between the K# and Cl they observed is in fact due to variation of the Cl concentration of the evolved brines. However, this would require the more K-rich bulk compositions to evolve more concentrated $FeCl_2$ brines than their Na-rich counterparts involving a process that is not obvious at this time.

Considering all the conflicting data regarding compositional constraints on Cl incorporation, further research is needed. One approach to better understand the compositional constraints on Cl uptake into amphiboles is to determine how the amphibole's structure responds to increasing amounts of Cl. This is difficult using naturally occurring amphiboles due to their large compositional variability and a lack of data for amphiboles with Cl content $> \sim 1.2$ apfu. Ideally, amphibole composition should be held constant while only varying the Cl content. This study uses electron microprobe analysis and Rietveld refinements to determine the chemical compositions and unit cell parameters, respectively, of a suite of 25 amphiboles, with Cl contents ranging from 0.0 to ~ 1.7 apfu. The Fe^{3+} fraction was determined using Mössbauer spectroscopy ($Fe^{3+}/Fe_{Total} \pm 5\,\%$) for all amphiboles in this study, so their compositions are well constrained. This research helps to better understand the physical processes of Cl incorporation into amphiboles, especially Cl-rich amphiboles (amphiboles with > 1.2 apfu Cl). Furthermore, trends between amphibole composition and unit cell volume are extrapolated using multivariate regression to derive the molar volume of, for example, ideal potassic-chloro-hastingsite (PCH_i) and other chloro-amphiboles, which can be used for later thermodynamic modeling.

2 Methods

2.1 Sample preparation

Reagents used consisted of silicic acid hydrate, aluminum oxide, ferric oxide, powdered metallic iron, magnesium oxide, calcium carbonate, potassium carbonate, sodium carbonate, and ferrous chloride. Amphibole-equivalent mixtures were prepared by combining the reagents in proportion to their theoretical end-member bulk composition. Because of the well-known non-stoichiometry of wüstite ($Fe_{1-x}O$, e.g., Waychunas, 1991), the chemical equivalent of FeO was achieved by mixing Fe_2O_3 and fine-grained ($\sim 10\,\mu m$) metallic iron (Fe°). The silicic acid hydrate was heated in air to 1100 °C at 1 atm (1 bar) to convert it into anhydrous silicon dioxide (usually cristobalite). All non-ferrous materials were

combined, mixed under ethanol, and heated in a 900 °C furnace for 15 min, both to decarbonate the Na_2CO_3, K_2CO_3, and $CaCO_3$ by reaction with SiO_2 and convert the mixture into a partial-glass assemblage to enhance its reactivity. The decarbonated mixture was weighed immediately upon cooling, and the weight value was used to correct the amounts of the remaining ferrous materials needed. The Fe_2O_3 and Fe° were then added and homogenized under ethanol.

In some experiments, specifically the "HastZ" series (Tables 1, 2), amphiboles were synthesized in $FeCl_2$ brines ranging from 1–100 m. For these runs, a mixture was assembled equivalent in composition to $KCa_2(Fe^{2+},Mg)_4Fe^{3+}Al_2Si_6O_{23}$, to which a mixture of $FeCl_2$ and deionized water (^DH_2O, < 1 part per million (ppm) Cl via ion chromatography) was added, sufficient to yield a desired brine $FeCl_2$ concentration at a brine / rock ratio of 0.2 / 1.0. For further discussion of the methodology for preparing these samples, see Matteucci et al. (2024). In all other Cl-containing bulk compositions, $FeCl_2$ was added last to the oxide mixture and homogenized dry for 15 min. For these samples, anhydrous conditions were desired during treatment to maximize Cl uptake by the amphibole. All bulk compositions explored in this study are listed in Table 1.

Starting mixtures were placed into capsules made of either Au or $Ag_{50}Pd_{50}$ alloy with outer diameters (ODs) from 4.0 to 5.0 mm. For double-capsule experiments, the outer capsule was made of 5.0 mm Au tubing and the inner from 4.0 mm $Ag_{50}Pd_{50}$ tubing. For all other experiments except HastO1-1, which used Au, starting mixtures were loaded into 4.0 mm $Ag_{50}Pd_{50}$ capsules. $Ag_{50}Pd_{50}$ capsules were used instead of Pt to minimize Fe uptake by the capsule (Driscall et al., 2005). In addition, $Ag_{50}Pd_{50}$ capsules maximized amphibole yields at a given set of P–T–f_{O_2} conditions when compared to more Ag-rich alloys (Jenkins, 2019). Au capsules were used when H_2 exchange was unwanted between the capsule and its environment, mainly to prevent formation of H_2O in the capsule by reaction of hydrogen with any excess oxygen. For mixtures containing $FeCl_2$, the loaded capsule was heated in air to 160 °C for 15 min prior to sealing to drive away moisture absorbed by this hygroscopic salt during reagent homogenization. However, some absorbed water is always present in the $FeCl_2$, making totally anhydrous conditions impossible to attain with these methods. For experiments that required a brine, ^DH_2O was added to the capsule using a microsyringe after heating the loaded capsule to 160 °C. Capsules were then immediately sealed by arc welding beneath a lightly moistened tissue, which helped reduce exposure of the AgPd melt to oxygen (Weidner, 1989).

2.2 Apparatus

2.2.1 Gas vessel

Experiments performed in internally heated gas vessels used argon or argon–hydrogen gas mixtures as the pressure medium. Two Inconel-sheathed chromel–alumel thermocouples were used to measure the thermal gradient along the length of the capsule during each experiment. Capsules were placed inside a hollow copper cylinder to reduce thermal gradients and to hold the samples in place near the thermocouple tips. Pressures were measured using both a Bourdon tube and factory-calibrated manganin pressure cell. Pressure uncertainties are ±0.005 GPa.

The f_{O_2} was controlled in one of two ways for gas vessel runs. One method followed the procedure as described in Matteucci et al. (2024), which uses a H_2–Ar mixture as the pressure medium. $Ag_{50}Pd_{50}$ capsules were used for all these runs. The other method uses the double-capsule method described in Eugster (1957). The buffering assemblage was Ni–NiO plus H_2O contained in an outer Au capsule, while $Ag_{50}Pd_{50}$ was used for the inner capsules. Double-capsule setups were pressurized only with Ar. For gas vessel runs, the double-capsule technique was only used for consistency with relevant piston cylinder runs as discussed in the next section. Treatment conditions were generally ∼ 700 °C and ∼ 0.3 GPa with durations ranging from 66–166 h. Samples were then quenched and weighed. Capsules were then punctured, weighed, subsequently heated to 110 °C for 15 min, and weighed again. This was done to quantify the volatiles present in the capsule after treatment.

2.2.2 Piston cylinder

Experiments requiring pressures above 0.4 GPa used a 0.5 in. diameter, non-end-loaded piston cylinder press. Single-sleeve NaCl cells were used as the pressure media in which the samples were imbedded. A single type K (chromel–alumel) thermocouple was used to measure the temperature at the top of the capsule. Hydraulic ram pressures were measured using a Heise Bourdon tube gauge. Sample pressure uncertainties of ±0.03 GPa were used for pressures ≥ 1.0 GPa (Quirion and Jenkins, 1998) and ±0.05 GPa for pressures between 0.5 and 1.0 GPa (Schneider and Jenkins, 2020). Since all capsules had an OD greater than 4.0 mm, a temperature uncertainty of ±15 °C was assumed (Schneider and Jenkins, 2020). Most experiments done in the piston cylinder were double capsules using the Ni–NiO oxygen buffer, as discussed in the previous section. However, two samples, PsBuff-1 and HastO1-1, were treated without a functional oxygen buffer (see below) to minimize capsule water accrual during treatment by hydrogen ingress. Therefore, removing the buffer should yield a more anhydrous environment with a higher Cl activity desired for forming chloro-amphiboles. HastO1-1 was synthesized in a gold capsule, while PsBuff-1 was synthesized in an $Ag_{50}Pd_{50}$ capsule using a pressure-medium buffer. More specifically, PsBuff-1 was an attempt to apply an oxygen buffer to a piston cylinder run by impregnating the ambient NaCl pressure media with Ni and NiO and assuming environmental H_2O from the pressure medium would react with it to impose a f_{H_2} on the

Table 1. List of bulk compositions explored in this study.

Sample code	Bulk composition
HastE-dP3k	$KCa_2(Fe^{2+}_4Fe^{3+})Al_2Si_6O_{22}Cl_2$ (PCH)
HastO1-1	$KCa_2(Fe^{2+}_{4.3}Fe^{3+}_{0.7})Al_2Si_6O_{21.85}Cl_2$ (PCH)
PsBuff-1	$KCa_2(Fe^{2+}_4Fe^{3+})Al_2Si_6O_{22}Cl_2$ (PCH)
ER-20kdc	$KCa_2(Fe^{2+}_4Fe^{3+})Al_2Si_6O_{22}Cl_2$ (PCH)
ER-15kdc	$KCa_2(Fe^{2+}_4Fe^{3+})Al_2Si_6O_{22}Cl_2$ (PCH)
ER-10kdc	$KCa_2(Fe^{2+}_4Fe^{3+})Al_2Si_6O_{22}Cl_2$ (PCH)
ER-5kdc	$KCa_2(Fe^{2+}_4Fe^{3+})Al_2Si_6O_{22}Cl_2$ (PCH)
ER-3kdc	$KCa_2(Fe^{2+}_4Fe^{3+})Al_2Si_6O_{22}Cl_2$ (PCH)
FR-830W	$KCa_2(Fe^{2+}_4Fe^{3+})Al_2Si_6O_{22}(OH)_2$ (PH)
HastZ-1*m*2	$KCa_2(Fe^{2+}_4Fe^{3+})Al_2Si_6O_{23}$ (PH) + 1 *m* $FeCl_2$ brine
HastZ-2*m*2	$KCa_2(Fe^{2+}_4Fe^{3+})Al_2Si_6O_{23}$ (PH) + 2 *m* $FeCl_2$ brine
HastZ-3*m*1	$KCa_2(Fe^{2+}_4Fe^{3+})Al_2Si_6O_{23}$ (PH) + 3 *m* $FeCl_2$ brine
HastZ-6*m*1	$KCa_2(Fe^{2+}_4Fe^{3+})Al_2Si_6O_{23}$ (PH) + 6 *m* $FeCl_2$ brine
HastZ-12*m*1	$KCa_2(Fe^{2+}_4Fe^{3+})Al_2Si_6O_{23}$ (PH) + 12 *m* $FeCl_2$ brine
HastZ-24*m*2	$KCa_2(Fe^{2+}_4Fe^{3+})Al_2Si_6O_{23}$ (PH) + 24 *m* $FeCl_2$ brine
HastZ-50*m*1	$KCa_2(Fe^{2+}_4Fe^{3+})Al_2Si_6O_{23}$ (PH) + 50 *m* $FeCl_2$ brine
HastZ-100*m*1	$KCa_2(Fe^{2+}_4Fe^{3+})Al_2Si_6O_{23}$ (PH) + 100 *m* $FeCl_2$ brine
HastZ0.75-12*m*1	$KCa_2(Fe^{2+}_3Mg\,Fe^{3+})Al_2Si_6O_{23}$ + 12 *m* $FeCl_2$ brine
HastZ0.5-12*m*2	$KCa_2(Fe^{2+}_2Mg_2Fe^{3+})Al_2Si_6O_{23}$ + 12 *m* $FeCl_2$ brine
PFS-3k700-1	$KCa_2(Fe^{2+}_3Al_2)Al_3Si_5O_{22}Cl_2$ (PCFS)
NC-15k700	$NaCa_2(Fe^{2+}_4Fe^{3+})Al_2Si_6O_{22}Cl_2$ (CH)
NC-10k700	$NaCa_2(Fe^{2+}_4Fe^{3+})Al_2Si_6O_{22}Cl_2$ (CH)
NC-6k700	$NaCa_2(Fe^{2+}_4Fe^{3+})Al_2Si_6O_{22}Cl_2$ (CH)
NC-3k700	$NaCa_2(Fe^{2+}_4Fe^{3+})Al_2Si_6O_{22}Cl_2$ (CH)

Abbreviations: PCH – potassic-chloro-hastingsite, PH – potassic-hastingsite, PCFS – potassic-chloro-ferro-sadanagaite, CH – chloro-hastingsite. All sample codes beginning with "HastZ" were synthesized from variable concentrated $FeCl_2$ brines. The number before "*m*" in the sample code is the brine $FeCl_2$ concentration in molality. The number after "Z" in the sample code is the Fe#; no number indicates an Fe# of 1.0. In sample codes containing "k", the number before is the pressure in kilobars.

capsule, while HastO1-1 was truly unbuffered. Based on the minimal amount of H_2 ingress into the capsule and the resultant high Cl concentration of PsBuff-1, the pressure-medium buffering technique provided little, if any, oxygen buffering. Treatment conditions were 700–850 °C and 0.5–2.0 GPa and durations ranged from 36–72 h. After quenching each run, the capsules were soaked in $^{D}H_2O$ to dissolve any adherent NaCl and were then weighed.

2.2.3 Cold-seal vessel

One sample, HastE-dP3k, was treated in a cold-seal vessel composed of a nickel-based alloy, René 41, with an outer to inner diameter ratio of 3 : 0.7. Pressures were measured using Heise Bourdon tube gauges. Pressure uncertainties are ±0.005 GPa. Capsules were placed into the vessel cavity, which was then filled with $^{D}H_2O$. A filler rod, also composed of René 41, was added to reduce the volume of the vessel cavity and minimize water convection and resultant thermal gradients inside the vessel. The vessel was then put into a furnace and brought up to the desired pressure and temperature. The f_{O_2} conditions during these experiments, which were not controlled by the double-capsule technique, were measured to be near Ni–NiO using the methods of Taylor et al. (1992), as discussed in Matteucci et al. (2024). Conditions were 601 °C and 0.318 GPa with a duration of 168 h. The run was quenched by first cooling the vessel and then relieving the pressure.

2.3 Analytical methods

Powder X-ray diffraction (XRD) analysis was performed using a Panalytical Xpert PW3040 diffractometer. Powdered samples were mounted on a zero-background single crystal quartz plate. For unit cell analysis, small amounts (1 wt %–5 wt %) of synthetic halite were mixed with the sample before scanning to correct the sample displacement using the peak positions of halite ($a_o = 5.6401$ Å). Operating conditions were 40 kV and 20 mA using Cu$K\alpha$ radiation and fitted with a diffracted-beam graphite monochromator. All samples

Table 2. Summary of run conditions and products.

Sample code	Apparatus	T (°C)	P (GPa)	t (h)	f_{O_2}[a]	$FeCl_2$ (m)	Products	wt % Amph
HastE-dP3k	CS	601 (10)	0.318 (5)	168	NNO[b]	NA	Amph, An, Mt, Sylv, Qtz	70.3 (7)
HastO1-1	PC	850 (15)	2.05 (4)	48	–	NA	Amph, Cpx, Mt, Gt, Sylv, Qtz	81.7 (12)
PsBuff-1	PC	700 (15)	1.59 (5)	36	NNO[c]	NA	Amph, Cpx, Fay, Mt, Gt, Sylv, Qtz	67.0 (24)
ER-20kdc	PC	700 (15)	1.99 (3)	48	NNO[b]	NA	Amph, Cpx, Fay, Gt, Sylv, Qtz, Ann	55.0 (9)
ER-15kdc	PC	700 (15)	1.49 (3)	48	NNO[b]	NA	Amph, Gt, Sylv, Qtz	86.7 (10)
ER-10kdc	PC	700 (15)	1.01 (5)	48	NNO[b]	NA	Amph, An, Sylv, Qtz	93.6 (12)
ER-5kdc	PC	700 (15)	0.50 (7)	72	NNO[b]	NA	Amph, An, Mt, Sylv, Qtz	83.9 (8)
ER-3Kdc	GV	704 (6)	0.310 (6)	96	NNO[b]	NA	Amph, Cpx, Mt, Sylv, Qtz, San	54.5 (8)
ER-700s	GV	701 (8)	0.348 (6)	114	0.09	NA	Amph, Cpx, An, Mt, Sylv, Qtz	89.7 (12)
FR-830W	GV	830 (6)	0.305 (12)	66	−0.02	0.00	Amph, Cpx, An, Mt, Sylv	76.2 (11)
HastZ-1m2	GV	701 (5)	0.300 (5)	96	0.02	1.12 (3)	Amph, Cpx, An, Mt, Sylv	76.2 (11)
HastZ-2m2	GV	701 (8)	0.305 (5)	96	0.02	1.90 (6)	Amph, Cpx, An, Mt, Sylv	83.3 (10)
HastZ-3m1	GV	700 (4)	0.300 (5)	96	0.02	2.60 (7)	Amph, Cpx, An, Mt, Sylv	84.2 (7)
HastZ-6m1	GV	700 (6)	0.304 (5)	96	0.01	7.54 (30)	Amph, An, Mt, Sylv	89.0 (11)
HastZ-12m1	GV	700 (2)	0.302 (5)	96	0.00	11.65 (58)	Amph, Cpx, An, Mt, Qtz, Sylv, Rkn	80.9 (9)
HastZ-24m2	GV	701 (2)	0.308 (5)	96	0.00	24.5 (21)	Amph, Cpx, An, Mt, Qtz, Rkn	71.9 (10)
HastZ-50m1	GV	700 (2)	0.298 (5)	96	0.02	43.1 (63)	Amph, Cpx, An, Fay, Qtz	78.0 (8)
HastZ-100m1	GV	687 (2)	0.305 (5)	96	−0.03	62.0 (128)	Amph, Cpx, An, Fay, Qtz	78.9 (7)
HastZ0.75-12m1	GV	700 (1)	0.315 (30)	96	−0.01	12.82 (68)	Amph, Cpx, Mt, Sylv, Rkn	80.6 (12)
HastZ0.5-12m2	GV	700 (3)	0.300 (5)	96	0.02	12.38 (71)	Amph, Cpx, An, Ol, Mt, San, Bt	26.7 (7)
PFS-3k700-1	GV	699 (7)	0.300 (5)	96	0.02	NA	Amph, Cpx, An, Mt, Qtz, Ann, Rkn	35.3 (10)
NC-15k700	PC	700 (15)	1.58 (4)	48	NNO[b]	NA	Amph, Cpx, Fay, Gt, Qtz, Ht	40.1 (6)

Table 2. Continued.

Sample code	Apparatus	T (°C)	P (GPa)	t (h)	f_{O_2} [a]	$FeCl_2$ (m)	Products	wt % Amph
NC-10k700	PC	700 (15)	1.03 (4)	48	NNO[b]	NA	Amph, Cpx, Gt, Ht, Rkn	77.8 (7)
NC-6k700	PC	700 (15)	0.60 (5)	96	NNO[b]	NA	Amph, Cpx, An, Qtz, Ht, Rkn	94.2 (11)
NC-3k700	GV	701 (7)	0.300 (5)	166	NNO[b]	NA	Amph, Cpx, An, Fay, Qtz, Ht, Rkn	81.2 (9)

Note: uncertainties (1σ) in the last digit in this and other tables are given in parentheses. Pressure uncertainties include both the precision of measurement and pressure variation during the experiment. $FeCl_2$ (m) values are the initial brine $FeCl_2$ concentrations for applicable samples. Amphibole concentration was determined by Rietveld refinement. Abbreviations: Ab – albite, An – anorthite, Ann – annite, Amph – amphibole, Bt – biotite, Cpx – hedenbergitic clinopyroxene, Fay – fayalite, Gt – garnet, Ht – halite, Mt – magnetite, NA – nominally anhydrous, Qtz – quartz, Rkn – rokühnite, San – sanidine, Sylv – sylvite, GV – gas vessel, PC – piston cylinder, and CS – cold-seal vessel. For GV runs, f_{O_2} was calculated using the P, T, and X_{H_2} of the pressure media. [a] Log oxygen fugacity relative to the Ni–NiO oxygen buffer of Frost (1991). [b] Double-capsule experiments with a Ni–NiO oxygen buffer. [c] Pressure medium impregnated with Ni and NiO.

were scanned from 5–60°2θ with a step size of 0.04° at 3 s per step. The divergent and anti-scatter slits had values of 1.0°. XRD data were analyzed by Rietveld refinements using the General Structure Analysis System (GSASII) software of Toby and Von Dreele (2013). The crystallographic information files (CIFs) used for refinements were almandine from Novak and Gibbs (1971), annite from Redhammer et al. (2000), anorthite from Angel (1988), fayalite from Smyth and Hazen (1973), halite from Walker et al. (2004), hastingsite from Makino et al. (1993), hedenbergite from Zhang et al. (1997), magnetite from Wechsler et al. (1984), quartz from Levien et al. (1980), sanidine from Ohashi and Finger (1974), rokühnite ($FeCl_2 \cdot 2H_2O$) from Morosin and Graeber (1965), and sylvite from Walker et al. (2004).

Several variables were allowed to vary during Rietveld refinement: background, sample displacement (using halite as a reference), unit cell parameters, phase fraction, preferred orientation, microstrain, and particle size. Site populations were fixed to the recalculated formulas as determined via EMPA for the amphiboles and pyroxenes. Site populations for the amphiboles were not refined because some samples had low concentrations of amphibole (< 50 %). While most samples had over a 70 % concentration, it was decided it is best to refine all samples identically for consistency.

All samples had their Fe^{3+} fraction determined via Mössbauer spectroscopy by M. Darby Dyar of Mount Holyoke College. The methods used for Mössbauer spectroscopy in this study were the same as those used for an earlier study of hastingsitic amphiboles (Matteucci et al., 2024) and are described in detail in Mueller et al. (2017). Mössbauer spectra fitting parameters and crystallographic site distributions are shown in Table 3.

Electron microprobe analysis (EMPA) was done initially at Binghamton University, but equipment failure led to many samples being analyzed at Syracuse University (Table 4). Electron microprobe analysis at Binghamton University was done on a JEOL 8900 Superprobe. Samples were rinsed in $^{D}H_2O$ to remove salts that interfere with the epoxy-curing process before mounting in epoxy and being polished with a final diamond grit size of 0.5 µm. Operating conditions were 15 kV and 10 nA. Analyses were done using 10 s on peaks and 3 s on background for all elements except Cl, which used 30 s on peaks and 10 s on background. Wollastonite was the standard used for Ca, orthoclase for K, albite for Na, hematite for Fe, quartz for Si, corundum for Al, and reagent grade palladium chloride ($PdCl_2$) for Cl. Matrix corrections were made with the ZAF scheme.

Electron microprobe analysis at Syracuse University was done on a Cameca SXFive with a LaB_6 electron gun using powdered samples dispersed over polished graphite rods. The operating conditions were 15 kV and 20 nA using sanidine as the standard for K, jadeite for Na, diopside for Ca and Si, enstatite for Mg, fayalite for Fe, kyanite for Al, and tugtupite for Cl. Analyses were done using 20 s on peaks and 10 s on background for all elements except Cl, which used 40 s on peaks and 20 s on background. Matrix corrections were made with the ZAF scheme. Analyses were found to be comparable between the two instruments.

Cations and anions were assigned to one of five groups (A, B, C, T, W) in the general formula $AB_2C_5T_8O_{22}W_2$ by (i) having the sum $O + OH + Cl = 24$; (ii) using the Fe^{3+} fraction from Mössbauer analysis to convert the EMPA total FeO into Fe_2O_3 and FeO, and then using them to calculate total amounts of Fe^{2+} and Fe^{3+}; and (iii) adding sufficient OH so that ^{A}Ca is minimized ($^{A}Ca < 0.05$) while the sum of $OH + Cl \leq 2.00$ and the B- and C-group cations contain 2.00 and 5.00 atoms, respectively. The following procedure was adopted for assigning cations to groups: first, all Si is added to the T cations, and then Al is allocated to fill the occupancy; if $Si + Al < 8$, Fe^{3+} is added so that $\sum T = 8.00$. Second, the remaining Al and Fe^{3+} are assigned to C, to which Mg and Fe^{2+} are then added so that $\sum C = 5.00$ with all Mg being assigned to the C cations (Driscall et al., 2005). Third, the remaining Fe^{2+} is added to B, to which Ca is then added so

https://doi.org/10.5194/ejm-36-247-2024

Table 3. Mössbauer spectra fitting parameters, crystallographic site distributions of Fe, and bulk ferric iron fractions for amphiboles that were not already reported in Matteucci et al. (2024).

Site iron distribution	Parameter	Sample code								
		HastE-3KdP	HastO1-1	PsBuff-1	ER-20kdc	ER-15kdc	ER-10kdc	ER-5kdc	ER-3Kdc	ER-700s
Octahedral Fe^{3+}	IS	0.31	0.42	0.33	0.33	0.33	0.32	0.46	0.45	0.30
$M(2)$	QS	0.79	0.62	0.80	0.80	0.85	0.91	0.62	0.62	0.93
	Width	0.34	0.41	0.45	0.47	0.43	0.41	0.45	0.43	0.41
	Area	16	24	23	19	18	21	24	17	21
Octahedral Fe^{2+}	IS	1.16	1.08	1.13	1.15	1.16	1.16	1.05	1.10	1.16
$M(4)$	QS	1.79	2.13	1.86	1.88	1.84	1.91	2.07	2.12	1.92
	Width	0.38	0.26	0.40	0.31	0.38	0.39	0.36	0.46	0.41
	Area	10	11	4	11	15	20	15	20	24
Octahedral Fe^{2+}	IS	1.17	1.10	1.17	1.15	1.14	1.14	1.11	1.13	1.15
$M(2)$	QS	2.23	2.42	2.19	2.25	2.23	2.32	2.45	2.49	2.34
	Width	0.31	0.26	0.34	0.30	0.30	0.30	0.30	0.30	0.29
	Area	19	24	17	22	21	27	31	18	27
Octahedral Fe^{2+}	IS	1.14	1.10	1.10	1.12	1.12	1.12	1.13	1.14	1.13
$M(1)$ $M(3)$	QS	2.66	2.65	2.60	2.62	2.63	2.67	2.76	2.82	2.70
	Width	0.30	0.26	0.31	0.32	0.33	0.30	0.24	0.25	0.27
	Area	26	27	26	42	39	32	21	11	28
$\%Fe^{3+}$		29.3	27.8	33.1	20.0	19.1	21.0	27.0	25.4	21.2
		FR-830W	HastZ0.75-12m1	HastZ0.5-12m2	PFS-3k700-1	NC-15k700	NC-10k700	NC-6k700	NC-3k700	
Octahedral Fe^{3+}	IS	0.37	0.44	0.44	0.40	0.40	0.34	0.42	0.42	
$M(2)$	QS	0.80	0.60	0.54	0.68	0.56	0.60	0.49	0.53	
	Width	0.47	0.43	0.36	0.53	0.34	0.48	0.49	0.54	
	Area	13	21	7	29	18	24	24	26	
Octahedral Fe^{2+}	IS	1.05	1.05	1.12	1.03	1.14	1.14	1.10	1.09	
$M(4)$	QS	1.72	2.06	2.34	1.83	2.04	2.04	2.14	1.95	
	Width	0.32	0.40	0.62	0.62	0.34	0.31	0.35	0.30	
	Area	3	13	43	23	23	19	27	15	
Octahedral Fe^{2+}	IS	1.17	1.12	1.14	1.10	1.13	1.11	1.10	1.11	
$M(2)$	QS	2.19	2.46	2.73	2.39	2.44	2.52	2.50	2.45	
	Width	0.40	0.30	0.26	0.35	0.26	0.31	0.25	0.29	
	Area	20	21	17	25	24	43	37	36	
Octahedral Fe^{2+}	IS	1.12	1.14	1.17	1.13	1.14	1.13	1.13	1.14	
$M(1)$ $M(3)$	QS	2.67	2.77	2.95	2.69	2.75	2.78	2.71	2.77	
	Width	0.32	0.26	0.26	0.26	0.24	0.26	0.26	0.26	
	Area	11	22	18	14	20	13	22	23	
$\%Fe^{3+}$		26.6	27.1	8.5	31.7	21.4	24.3	21.9	26.3	

Abbreviations: IS – isomer shift (mm s^{-1}); QS – quadrupole splitting (mm s^{-1}). Width is the full width at half maximum (mm s^{-1}), while the area is given as the percentage of the total peak area in each doublet.

Table 4. Compositions of amphiboles synthesized in this study that were not already reported in Matteucci et al. (2024).

Experiment name	HastE-3KdP	HastO1-1	PsBuff-1	ER-20kdc	ER-15kdc	ER-10kdc
n	26	27	9	18	24	21
SiO_2	34.18 (283)	31.86 (340)	34.77 (299)	37.23 (203)	36.90 (267)	35.58 (352)
Al_2O_3	9.24 (120)	6.69 (60)	8.96 (227)	7.21 (81)	9.09 (134)	9.22 (94)
FeO	22.28 (179)	24.05 (282)	21.37 (99)	26.39 (125)	26.05 (141)	25.30 (166)
Fe_2O_3	10.26 (82)	10.32 (298)	11.74 (54)	7.33 (35)	6.84 (37)	7.46 (49)
MgO	–	–	–	–	–	–
CaO	10.05 (79)	9.26 (88)	10.27 (114)	10.30 (59)	10.16 (63)	9.89 (74)
Na_2O	–	–	–	–	–	–
K_2O	3.17 (43)	3.70 (35)	3.93 (53)	4.09 (21)	3.76 (26)	3.41 (27)
Cl	2.53 (33)	5.14 (49)	5.24 (58)	4.89 (29)	3.97 (35)	3.96 (39)
H_2O[a]	0.46 (24)	0.08 (10)	0.00 (0)	0.00 (0)	0.22 (15)	0.29 (16)
Total	90.67 (679)	89.98 (666)	95.11 (768)	96.72 (485)	96.08 (530)	94.08 (724)
Unit formulae						
^{T}Si	6.24 (16)	6.15 (28)	6.21 (24)	6.60 (7)	6.47 (16)	6.36 (18)
^{T}Al	1.75 (15)	1.53 (14)	1.74 (28)	1.40 (7)	1.52 (15)	1.64 (17)
$^{T}Fe^{3+}$	0.01 (4)	0.32 (23)	0.04 (9)	0.00 (1)	0.00 (2)	0.00 (1)
Sum T	8.00	8.00	8.00	8.00	8.00	8.00
^{C}Al	0.24 (21)	0.00 (0)	0.12 (15)	0.11 (8)	0.36 (20)	0.31 (17)
$^{C}Fe^{3+}$	1.40 (16)	1.20 (31)	1.54 (17)	0.98 (12)	0.90 (12)	1.00 (13)
$^{C}Fe^{2+}$	3.36 (22)	3.80 (31)	3.19 (23)	3.90 (14)	3.74 (21)	3.69 (19)
^{C}Mg	–	–	–	–	–	–
Sum C	5.00	5.00	4.85 (9)	4.98 (2)	5.00	5.00
^{B}Fe	0.05 (5)	0.09 (8)	0.01 (4)	0.02 (3)	0.09 (5)	0.11 (5)
^{B}Ca	1.95 (5)	1.91 (8)	1.95 (7)	1.95 (4)	1.91 (5)	1.89 (5)
Sum B	2.00	2.00	1.96 (4)	1.97 (3)	2.00	2.00
^{A}Na	–	–	–	–	–	–
^{A}K	0.74 (6)	0.91 (4)	0.89 (6)	0.93 (3)	0.84 (4)	0.78 (5)
^{A}Ca	0.02 (2)	0.00 (1)	0.01 (1)	0.01 (1)	0.00 (0)	0.01 (1)
Sum A	0.75 (7)	0.91 (4)	0.90 (7)	0.93 (3)	0.85 (4)	0.79 (5)
Cations	15.75 (7)	15.92 (4)	15.72 (10)	15.89 (5)	15.84 (4)	15.79 (5)
Cl	0.78 (7)	1.68 (7)	1.58 (6)	1.47 (5)	1.18 (7)	1.20 (8)
OH	0.57 (32)	0.05 (10)	0.00 (0)	0.00 (0)	0.24 (21)	0.33 (24)
Anions	1.35 (33)	1.73 (17)	1.58 (17)	1.47 (13)	1.42 (25)	1.53 (29)
Fe^{3+}/Fe_{total}	0.293 (15)	0.278 (14)	0.331 (17)	0.200 (10)	0.191 (10)	0.210 (10)

that $\sum B = 2.00$. Finally, all K and Na along with any remaining Ca (which should be insignificant) are added to the A cations. Adding large amounts of OH has the effect of diluting and lowering the total cations so that OH can be balanced with the total A, B, and C cations to achieve a desirable amphibole formula, as described above. There is a "sweet spot" where, by adding OH, ^{A}Ca approaches 0 immediately before B- or C-group cations begin to fall below their required thresholds, which was the solution used when determining amphibole stoichiometry.

Analytical totals below 75 wt % were discarded as well as samples where B cations are < 2.00, C cations are < 5.00, and total cations are less than 15.00 or greater than 16.00. However, one sample (PsBuff-1) had persistently low B- and C-group cations, perhaps due to analytical error. Nonetheless, this sample was included in this study due to its very high Cl content and to motivate additional research into the possibility of B- and C-group vacancies in iron-rich amphiboles (Oberti et al., 2018). In addition, some of the highest-Cl amphiboles contained non-negligible amounts of tetrahedral Fe^{3+}, particularly HastO1-1, which had the most Cl of any amphibole from this study.

3 Results

3.1 Run products

Table 2 lists the run products, conditions, and amphibole concentration of each experimental charge. Furthermore, the initial $FeCl_2$ brine concentration, or brine concentration at the

Table 4. Continued.

Experiment name	ER-5kdc	ER-3Kdc[b]	ER-700s	FR-830W	HastZ0.75-12*m*1[b]	HastZ0.5-12*m*2
n	14	15	23	10	12	15
SiO_2	34.69 (417)	36.79 (233)	34.61 (333)	34.66 (166)	37.58 (260)	38.68 (271)
Al_2O_3	10.91 (167)	9.83 (71)	8.38 (125)	14.65 (78)	10.51 (121)	13.26 (162)
FeO	21.52 (186)	24.57 (126)	24.84 (137)	22.99 (65)	18.19 (124)	17.58 (127)
Fe_2O_3	8.84 (76)	9.31 (48)	7.43 (41)	9.26 (26)	7.51 (49)	1.85 (87)
MgO	–	–	–	–	4.47 (57)	6.93 (82)
CaO	9.88 (101)	10.50 (75)	9.23 (74)	10.89 (48)	10.01 (68)	10.06 (117)
Na_2O	–	–	–	–	–	–
K_2O	2.61 (24)	2.25 (19)	2.90 (32)	4.50 (21)	1.93 (23)	2.08 (55)
Cl	1.76 (21)	1.34 (15)	3.06 (35)	–	0.91 (10)	0.61 (6)
H_2O[a]	0.59 (15)	1.07 (17)	0.47 (19)	1.25 (10)	1.28 (16)	1.67 (14)
Total	89.32 (914)	93.67 (496)	89.70 (599)	96.02 (370)	90.36 (517)	90.84 (544)
Unit formulae						
^{T}Si	6.28 (16)	6.33 (14)	6.42 (25)	5.79 (8)	6.39 (13)	6.35 (14)
^{T}Al	1.72 (16)	1.67 (14)	1.58 (25)	2.21 (8)	1.61 (13)	1.65 (14)
$^{T}Fe^{3+}$	0.00 (0)	0.00 (0)	0.00 (0)	0.00 (0)	0.00 (0)	0.00 (0)
Sum T	8.00	8.00	8.00	8.00	8.00	8.00
^{C}Al	0.61 (18)	0.33 (15)	0.26 (15)	0.67 (9)	0.49 (20)	0.92 (13)
$^{C}Fe^{3+}$	1.21 (15)	1.21 (14)	1.04 (13)	1.17 (14)	0.96 (24)	0.23 (22)
$^{C}Fe^{2+}$	3.18 (20)	3.47 (18)	3.70 (18)	3.16 (16)	2.40 (24)	2.15 (24)
^{C}Mg	–	–	–	–	1.14 (16)	1.70 (22)
Sum C	5.00	5.00	5.00	5.00	5.00	5.00
^{B}Fe	0.09 (7)	0.07 (6)	0.17 (8)	0.05 (4)	0.18 (5)	0.26 (14)
^{B}Mg	–	–	–	–	0.00 (0)	0.00 (0)
^{B}Ca	1.91 (7)	1.93 (6)	1.83 (8)	1.95 (4)	1.82 (5)	1.74 (14)
Sum B	2.00	2.00	2.00	2.00	2.00	2.00
^{A}Na	–	–	–	–	–	–
^{A}K	0.61 (5)	0.49 (3)	0.69 (7)	0.96 (2)	0.42 (4)	0.44 (15)
^{A}Ca	0.01 (1)	0.01 (1)	0.01 (2)	0.00 (0)	0.01 (0)	0.03 (2)
Sum A	0.62 (5)	0.51 (3)	0.70 (7)	0.96 (2)	0.42 (4)	0.46 (15)
Cations	15.62 (5)	15.51 (3)	15.70 (7)	15.96 (2)	15.42 (3)	15.47 (14)
Cl	0.55 (8)	0.39 (4)	0.96 (9)	–	0.26 (3)	0.17 (2)
OH	0.72 (20)	1.23 (21)	0.60 (26)	1.40 (14)	1.46 (22)	1.83 (8)
Anions	1.27 (26)	1.62 (25)	1.56 (30)	1.40 (20)	1.72 (31)	2.00 (21)
Fe^{3+}/Fe_{total}	0.270 (14)	0.254 (13)	0.212 (11)	0.266 (13)	0.271 (14)	0.085 (4)

start of treatment, is listed for applicable samples. Samples containing $FeCl_2$ without added water are referred to as nominally anhydrous (NA), indicating that any water present in the capsule is incidental, as previously discussed. Coexisting phases are typically hedenbergite clinopyroxene, fayalite and/or magnetite, plagioclase, quartz, and sylvite/halite. At pressures of 1.0 GPa and greater, garnet forms instead of plagioclase. A form of hydrated $FeCl_2$ is likely present in all Cl-containing samples but only appears on XRD scans (typically as $FeCl_2 \cdot 2H_2O$) when the lab dew point is below its deliquescence point. Additionally, Cl-bearing biotite is present in some samples, especially in more Mg-rich bulk compositions.

3.2 Effects of pressure

The effect of pressure on Cl incorporation into amphiboles was investigated here, expanding upon the range explored by Jenkins (2019) (0.2–0.45 GPa). Endmember potassic-chloro-hastingsite and chloro-hastingsite were synthesized from 0.3–2.0 GPa. Both Na and K hastingsites were investigated to determine if the type of A cation affected the relationship between pressure and Cl. Samples were treated in a double-capsule setup using the Ni–NiO oxygen buffer. This was the only consistent way to buffer the oxygen fugacity between the different apparatuses required for the broad pressure ranges explored. Amphibole yield for these runs was generally good ($> 75\,\%$) but dropped off as the pressure was raised above ~ 1.0 GPa, especially for the chloro-hastingsite.

Table 4. Continued.

Experiment name	PFS-3k700-1[b]	NC-15k700[b]	NC-10k700[b]	NC-6k700[b]	NC-3k700[b]
n	16	14	16	19	29
SiO_2	30.11 (342)	34.05 (255)	36.19 (260)	35.75 (328)	35.59 (205)
Al_2O_3	15.35 (338)	7.79 (169)	10.08 (274)	9.41 (129)	9.80 (141)
FeO	18.87 (156)	25.96 (118)	25.94 (284)	24.99 (165)	23.78 (110)
Fe_2O_3	9.71 (83)	7.84 (89)	9.14 (154)	9.20 (99)	9.43 (60)
MgO	–	–	–	–	–
CaO	8.93 (113)	8.56 (90)	9.04 (59)	9.47 (118)	9.93 (66)
Na_2O	–	2.53 (35)	2.53 (34)	2.34 (28)	2.14 (21)
K_2O	3.35 (42)	–	–	–	–
Cl	3.31 (37)	3.90 (51)	4.13 (36)	3.77 (46)	3.46 (22)
H_2O[a]	0.25 (20)	0.24 (15)	0.13 (10)	0.34 (12)	0.27 (14)
Total	88.65 (806)	89.84 (526)	96.14 (512)	94.00 (630)	93.21 (409)
Unit formulae					
^{T}Si	5.58 (29)	6.38 (22)	6.29 (27)	6.32 (22)	6.30 (10)
^{T}Al	2.42 (29)	1.58 (20)	1.71 (26)	1.67 (21)	1.70 (10)
$^{T}Fe^{3+}$	0.00 (0)	0.04 (7)	0.00 (0)	0.01 (5)	0.00 (0)
Sum T	8.00	8.00	8.00	8.00	8.00
^{C}Al	0.92 (36)	0.14 (22)	0.35 (30)	0.29 (14)	0.34 (24)
$^{C}Fe^{3+}$	1.36 (21)	1.07 (24)	1.20 (42)	1.07 (24)	1.26 (13)
$^{C}Fe^{2+}$	2.71 (33)	3.79 (24)	3.46 (48)	3.64 (22)	3.40 (18)
^{C}Mg	–	–	–	–	–
Sum C	5.00	5.00	5.00	5.00	5.00
^{B}Fe	0.22 (19)	0.28 (13)	0.32 (9)	0.22 (14)	0.12 (6)
^{B}Ca	1.78 (19)	1.72 (13)	1.68 (9)	1.78 (14)	1.88 (6)
Sum B	2.00	2.00	2.00	2.00	2.00
^{A}Na	–	0.92 (12)	0.85 (9)	0.80 (10)	0.74 (6)
^{A}K	0.79 (7)	–	–	–	–
^{A}Ca	0.00 (0)	0.00 (0)	0.00 (0)	0.01 (1)	0.01 (0)
Sum A	0.79 (7)	0.92 (12)	0.85 (9)	0.81 (10)	0.74 (6)
Cations	15.80 (7)	15.92 (12)	15.85 (9)	15.81 (10)	15.74 (6)
Cl	1.05 (11)	1.24 (14)	1.22 (10)	1.13 (13)	1.04 (6)
OH	0.28 (27)	0.25 (22)	0.09 (12)	0.36 (17)	0.32 (18)
Anions	1.33 (32)	1.49 (35)	1.31 (37)	1.49 (29)	1.36 (23)
Fe^{3+}/Fe_{total}	0.317 (16)	0.214 (22)	0.243 (46)	0.219 (23)	0.263 (6)

Note: analyses reported as weight percent of the oxides and cations per O + Cl + OH = 24 of the average of *n* electron microprobe analyses. The ferric iron proportion was determined via Mössbauer analysis. [a] H_2O was estimated by minimizing ^{A}Ca and barring K from the B-group cations. [b] Samples analyzed at Syracuse University.

Figure 1 shows the correlations between pressure and ^{T}Al, $^{C}Fe^{2+}$, *A*-site occupancy, and Cl. They all display positive correlations except for ^{T}Al, which has a negative correlation. Additionally, there is a difference in pressure sensitivity among the four compositional components. For both Cl and the *A*-site occupancy, K-hastingsites (PCH) are more sensitive to pressure variation than Na-hastingsites (CH), whereas for $^{C}Fe^{2+}$ and ^{T}Al both amphibole groups show a similar response to pressure variation.

3.3 General compositional correlations

The amphiboles of this study are divided into four groups based on the bulk composition of their starting material. They are as follows: (1) PCHvCl – potassic-hastingsite ($KCa_2(Fe_4Fe^{3+})(Al_2Si_6)O_{22}(OH,Cl,O)_2$) with variable Cl content, ranging from 0.0–1.68 apfu; (2) PCHvFe – potassic-hastingsite ($KCa_2((Fe,Mg)_4Fe^{3+})(Al_2Si_6)O_{22}(OH,Cl,O)_2$) synthesized in constant 12 *m* $FeCl_2$ brines with variable Fe#, ranging from 0.5 to 1.0; (3) PCFS – potassic-chloro-ferro-sadanagaite ($KCa_2(Fe_3Al_2)(Al_3Si_5)O_{22}(OH,Cl,O)_2$); and (4) CHvCl – chloro-hastingsite ($NaCa_2(Fe_4Fe^{3+})(Al_2Si_6)O_{22}(OH,Cl,O)_2$) with variable Cl content, ranging from 1.04–

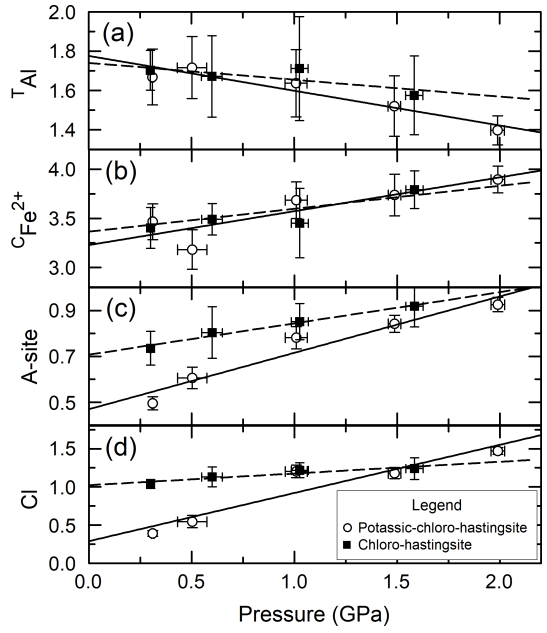

Figure 1. Effect of pressure on amphibole composition. The components shown, in atoms per formula unit, are **(a)** tetrahedral Al, **(b)** octahedral Fe^{2+}, **(c)** *A*-site occupancy, and **(d)** Cl content. Open circles are potassic-chloro-hastingsite (PCH); solid squares are chloro-hastingsite (CH). Solid lines are linear regression to the PCH data; dashed lines are linear regression to the CH data.

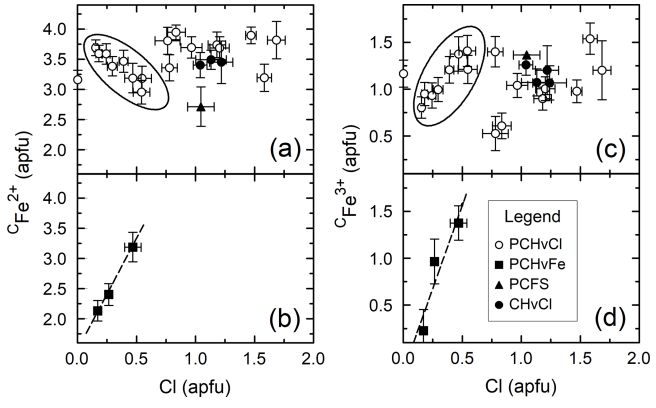

Figure 2. **(a)** Cl vs. $^{C}Fe^{2+}$ for Mg-free amphiboles; **(b)** Cl vs. $^{C}Fe^{2+}$ for amphiboles with variable Fe#. **(c)** Cl vs. $^{C}Fe^{3+}$ for Mg-free amphiboles; **(d)** Cl vs. $^{C}Fe^{3+}$ for amphiboles with variable Fe#. Lines are linear regressions to the data. Circles indicate amphiboles synthesized in increasingly concentrated $FeCl_2$ brines (from left to right).

1.24 apfu. The compositions of the amphiboles synthesized in this study are listed in Table 4. Subdividing the amphiboles into these groups allows a more convenient analysis of the crystal chemical trends in compositionally complex minerals like amphiboles.

Figure 2 shows the correlation between $^{C}Fe^{2+}$ and Cl (panels a and b) and the correlation between $^{C}Fe^{3+}$ and Cl (panels c and d) for Mg-free amphiboles (panels a and c), and variable Fe# amphiboles (panels b and d). When the Fe# of the bulk composition is held constant, no clear trend is observed between either Fe^{2+} or Fe^{3+} and Cl, excluding the circled areas of Fig. 2a and c, which represent amphiboles synthesized in brines with variable $FeCl_2$ concentration. For these latter samples, the negative correlation between $^{C}Fe^{2+}$ and Cl and positive correlation between $^{C}Fe^{3+}$ and Cl are associated with increasingly concentrated $FeCl_2$ brines elevating the ferric iron fraction of the amphiboles. These correlations are caused by variation in the brine Cl concentration as the dominant factor influencing the Cl concentration of the amphibole as discussed in detail in Matteucci et al. (2024). When the Fe# of the bulk composition is varied (Fig. 2b and d), $^{C}Fe^{2+}$ and $^{C}Fe^{3+}$ are positively correlated with Cl indicating that the substitution of $^{C}Fe^{2+,3+}$ for ^{C}Mg aids Cl incorporation in the structure. While the substitution of $^{C}Fe^{2+}$ for ^{C}Mg is charge conservative, the substitution of $^{C}Fe^{3+}$ for ^{C}Mg likely operates via the coupled substitution $^{C}Mg + {}^{O(3)}OH^{-} \leftrightharpoons {}^{C}Fe^{3+} + {}^{O(3)}O^{2-}$, as indicated by the negative correlation between ^{C}Mg and $^{O(3)}O$ in Fig. 3. Please note that all $^{O(3)}O$ values are calculated and have not been confirmed via direct measurement. Although the amphiboles for all groups except PCHvFe were synthesized from Mg-free starting mixtures, there is still moderate variation in the amount of $^{C}Fe^{2+}$, which is not well correlated with Cl on Fig. 2a or c. Comparing Fig. 2a and c to Fig. 4a, which shows the total octahedral iron ($^{C}Fe_{Total}$) vs. Cl for Mg-free amphiboles, it is apparent that $^{C}Fe_{Total}$ has a weak positive correlation with Cl. A stronger positive correlation is present between $^{C}Fe_{Total}$ and Cl in Fig. 4b, which shows amphiboles with variable Fe#. Comparison of the slope of the Mg-free amphiboles (Fig. 4a) to the variable Fe# amphiboles (Fig. 4b) highlights differences in the degree of influence that different cation substitutions exert on Cl incorporation. Because the synthetic Mg-free hastingsites can only have Fe or Al as C cations, Fig. 4a reflects the substitution of $^{C}Fe^{2+,3+}$ for ^{C}Al. The substitution of $^{C}Fe^{3+}$ for $^{C}Al^{3+}$ is charge conservative, while substitution of Fe^{2+} for Al^{3+} would require a coupled substitution such as $^{C}Fe^{2+} + {}^{T}Si^{4+} \leftrightharpoons {}^{C}Al^{3+} + {}^{T}Al^{3+}$ or $^{C}Fe^{2+} + {}^{O(3)}OH^{-} \leftrightharpoons {}^{C}Al^{3+} + {}^{O(3)}O^{2-}$ to maintain charge balance. While these reactions that substitute Fe for Al exert a modest control on Cl content (Fig. 4a), the preponderance of data from natural amphiboles and the steeper line of Fig. 4b compared to Fig. 4a affirm the importance of the exchange of $Fe^{2+,3+}$ for Mg on Cl incorporation. All data indicate that Fe is the preferred octahedral cation of Cl-rich amphiboles. Another noteworthy observation that supports the previous argument is the extremely low total aluminum in the most Cl-rich samples (Table 4). It is so low, in fact, that there is sometimes insufficient Al to fill the *T* sites, suggesting the presence of $^{T}Fe^{3+}$. The most Cl-rich sample (HastO-1) also has the lowest total Al and, therefore, the most $^{T}Fe^{3+}$.

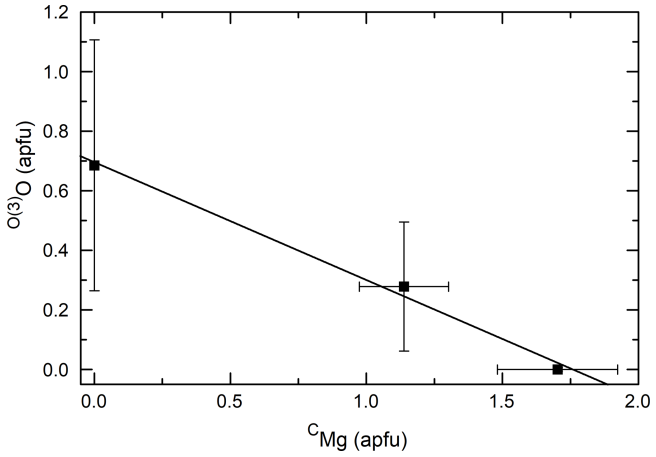

Figure 3. ^{C}Mg vs. $^{O(3)}$O for variable Fe# amphibole. Line is a linear regression to the data.

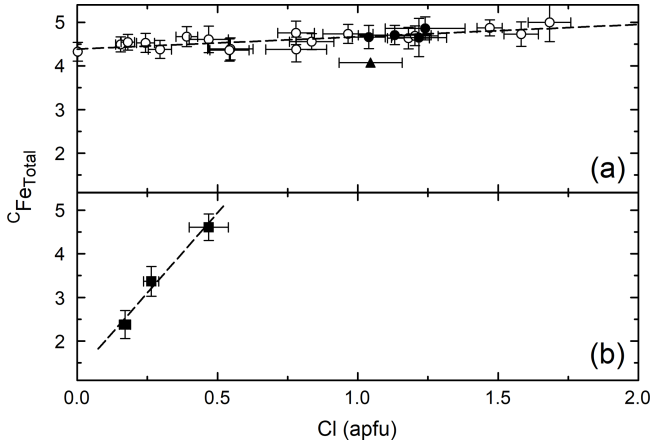

Figure 4. Cl vs. ^{C}Fe$_{Total}$ for Mg-free amphiboles **(a)** and variable Fe# amphiboles **(b)**. Lines are linear regressions to the data, excluding PCFS (triangle) in **(a)**. Symbols are the same as in previous figures.

Figure 5 shows the relationship between the Cl content and the *A*-site occupancy of the amphiboles of this study. Overall, the correlation is positive, though a few samples, particularly those synthesized in dilute $FeCl_2$ brines (0–6 *m*, below $\sim$0.35 Cl apfu), display a negative correlation. This is due to the $A^+ + {}^{C}Fe^{2+} \leftrightharpoons {}^{A}\square + {}^{C}Fe^{3+}$ substitution, in which a negative correlation between the Cl content and the *A*-site occupancy is a function of increasing $^{C}Fe^{3+}$ caused by increasingly concentrated $FeCl_2$ brines. For these samples, the increasing brine $FeCl_2$ concentration is acting both to increase the Cl content of the amphiboles and further oxidize the iron (Matteucci et al., 2024). Excluding these outliers, amphiboles of all four groups form a single trend suggesting a strong relation between the *A*-site occupancy and the Cl content.

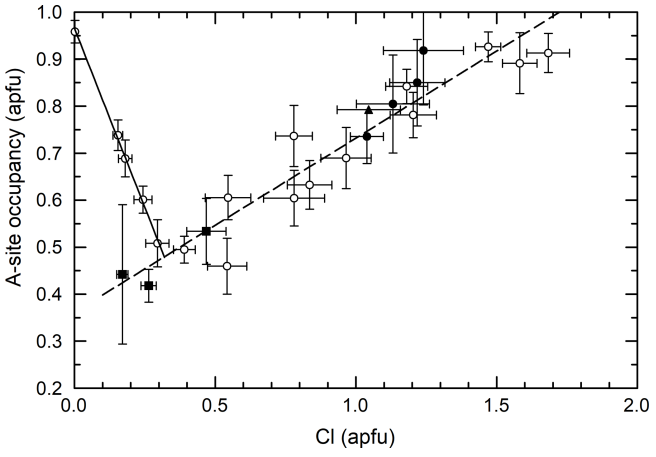

Figure 5. Cl vs. *A*-site occupancy of analyzed amphiboles. Generally, there is a positive correlation. However, the low Cl amphiboles synthesized in dilute $FeCl_2$ brines display a negative correlation, which inverts to positive at $\sim$0.35 apfu Cl. Trend lines are linear regressions to the PCHvCl data (open circles). Symbols are the same as in previous figures.

3.4 Unit cell – composition relations

Unit cell parameters were determined by Rietveld refinements and are listed in Table 5. Unit cell parameters are compared to amphibole compositions, and relevant trends are shown in Figs. 6–9. These diagrams are presented simply to illustrate observed correlations; variations in the unit cell parameters are not solely attributed to the compositional variable being shown. The multiple regression given in the Discussion section will provide a better assessment of compositional influences on a given parameter. Note that figures were only included when correlations were present; no correlations were present involving $^{C}Fe^{3+}$ or the *T* cations.

Figure 6 shows the dependence of unit cell parameters on the Cl content of amphibole. As expected, Cl expands the lattice, due to its large ionic radius (1.81 Å) when compared to OH^- (1.37 Å) and O^{2-} (1.40 Å) (Shannon, 1976). However, due to the complex composition of amphiboles, other atomic substitutions (^{T}Al for ^{T}Si, $^{A}\square$ for A^+, $^{C}Fe^{2+}$ for ^{C}Mg) also affect the unit cell parameters, adding some complexity to the trends. For the PCHvCl amphiboles (open circles), the trend between *a* and Cl is very similar to the trend between *A*-site occupancy and Cl (Fig. 5). Furthermore, the *a* parameters of Na-amphiboles (solid circles) are $\sim$0.1 Å smaller than the K-amphiboles on average, consistent with the smaller ionic radius of Na^+ (1.39 Å) compared to K^+ (1.64 Å) (Shannon, 1976). The correlation between *b* and Cl is good and nearly colinear for the PCHvCl and CHvCl amphiboles. The PCHvFe amphiboles also have a positive linear relationship, but with a steeper slope than the Mg-free samples. The correlation between *c* and Cl is good, and all samples are nearly colinear, though there are

Table 5. Unit cell parameters of amphiboles formed in this study.

Sample code	a (Å)	b (Å)	c (Å)	β (°)	V (Å^3)
HastE-dP3k	10.019 (4)	18.307 (1)	5.372 (1)	105.07 (7)	951.41 (88)
HastO1-1	10.027 (5)	18.404 (2)	5.378 (2)	104.89 (9)	959.09 (108)
PsBuff-1	10.032 (18)	18.386 (7)	5.386 (6)	104.89 (34)	960.08 (393)
ER-20kdc	10.048 (6)	18.397 (3)	5.367 (3)	104.87(12)	958.92 (132)
ER-15kdc	10.032 (4)	18.354 (2)	5.370 (1)	104.92 (7)	955.40 (91)
ER-10kdc	10.014 (5)	18.341 (2)	5.372 (2)	104.88 (9)	953.67 (106)
ER-5kdc	9.987 (4)	18.265 (1)	5.366 (1)	105.06 (7)	945.13 (81)
ER-3kdc	9.975 (5)	18.260 (2)	5.360 (1)	105.05 (9)	942.73 (103)
ER-700s	9.998 (5)	18.315 (2)	5.368 (2)	104.88 (9)	950.03 (111)
FR-830W	10.075 (7)	18.202 (3)	5.343 (2)	105.55 (14)	943.95 (178)
HastZ-1m2	10.033 (4)	18.235 (2)	5.348 (1)	105.29 (8)	943.85 (113)
HastZ-2m2	10.019 (4)	18.244 (2)	5.350 (1)	105.22 (7)	943.67 (89)
HastZ-3m1	10.004 (4)	18.253 (2)	5.352 (1)	105.14 (8)	943.38 (97)
HastZ-6m1	9.978 (4)	18.258 (2)	5.352 (1)	105.04 (8)	941.69 (98)
HastZ-12m1	9.976 (4)	18.268 (2)	5.357 (1)	104.98 (8)	943.10 (100)
HastZ-24m2	9.971 (5)	18.268 (2)	5.358 (2)	104.96 (10)	942.86 (114)
HastZ-50m1	9.976 (4)	18.284 (1)	5.365 (1)	104.96 (7)	945.54 (88)
HastZ-100m1	9.977 (3)	18.301 (1)	5.371 (1)	104.90 (6)	947.67 (78)
HastZ0.75-12m1	9.934 (5)	18.191 (2)	5.341 (2)	105.02 (10)	932.24 (126)
HastZ0.5-12m2	9.877 (9)	18.115 (4)	5.334 (3)	105.10 (18)	921.39 (218)
PFS-3k700-1	9.955 (12)	18.229 (4)	5.381 (4)	104.96 (22)	943.43 (251)
NC-15k700	9.866 (7)	18.361 (3)	5.371 (2)	103.98 (14)	944.09 (160)
NC-10k700	9.859 (4)	18.340 (1)	5.377 (1)	104.18 (8)	942.54 (88)
NC-5k700	9.864 (4)	18.331 (1)	5.379 (1)	104.32 (7)	942.41 (90)
NC-3k700	9.877 (4)	18.330 (2)	5.372 (1)	104.39 (8)	942.04 (95)

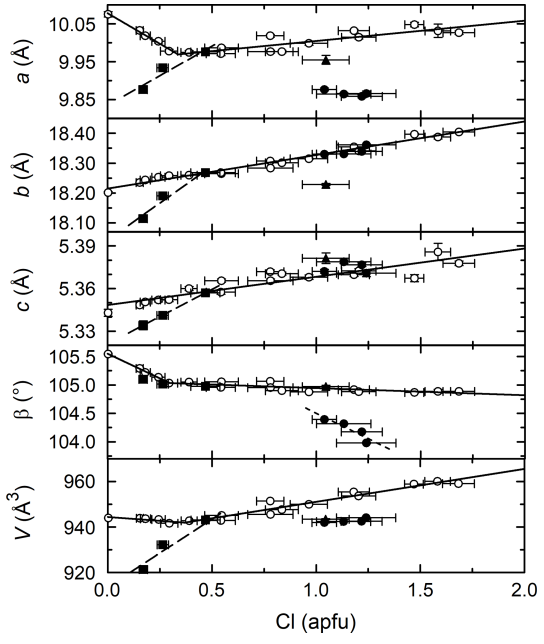

Figure 6. Amphibole Cl concentration vs. unit cell parameters. Solid lines are linear regressions to the PCHvCl data. Thick dashed lines are linear regressions to the PCHvFe data. The fine dashed line is a linear regression to the CHvCl data. Symbols are the same as in previous figures.

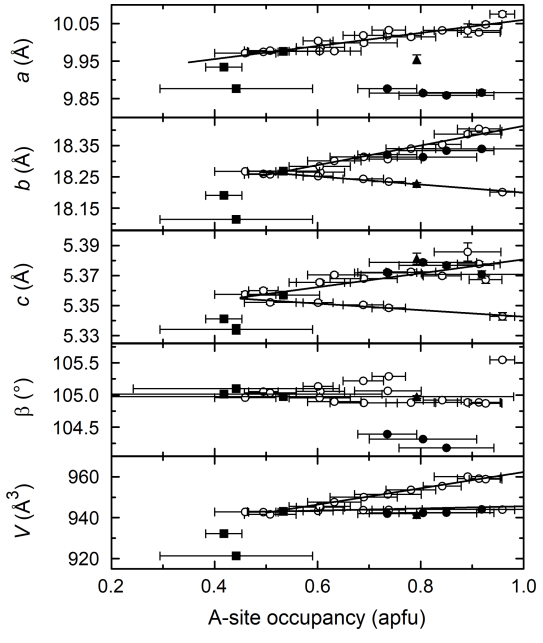

Figure 7. *A*-site occupancy vs. unit cell parameters. Trend lines are linear regressions to the PCHvCl data. Symbols are the same as in previous figures.

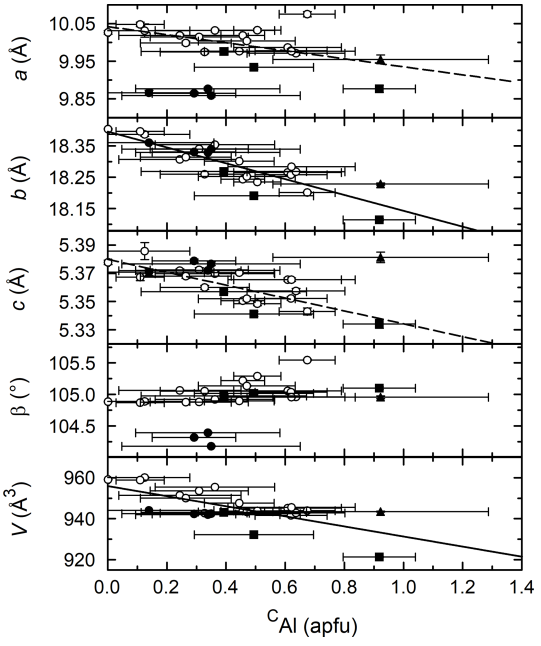

Figure 8. ^{C}Al vs. unit cell parameters. Solid lines are linear regressions to all the data. Dashed lines are linear regressions to the potassic hastingsites (open circles and solid squares). Symbols are the same as in previous figures.

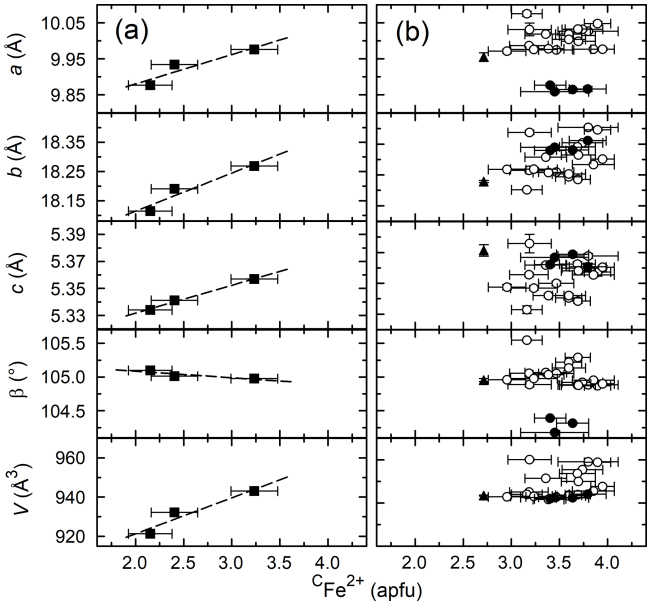

Figure 9. (a) $^{C}Fe^{2+}$ vs. unit cell parameters for the amphiboles formed with variable Fe# (PCHvFe data). Trend lines are linear regressions. **(b)** $^{C}Fe^{2+}$ vs. unit cell parameters for all other data. Symbols are the same as in previous figures.

also similarities to the *b*–Cl relationships, i.e., positive linear correlation, slightly steeper slope for PCHvFe amphiboles. Beta decreases with increasing Cl, especially when Cl $< \sim 0.35$ apfu. All amphibole groups are colinear on the β vs. Cl plot except for the Na amphiboles, which show a steeper-sloped negative correlation. Overall, unit cell volume increases with the Cl content of the amphibole, though it is complicated by the *A*-site occupancy, *A*-site cation, and Fe#.

Figure 7 shows the relationship between *A*-site occupancy and unit cell parameters. The best correlation is the positive linear relationship between *a* and *A* (*A*-site occupancy) for the PCHvCl and PCHvFe amphiboles; the CHvCl and PCFS amphiboles are outliers. Interestingly, while the K-amphiboles have a positive correlation between *a* and *A*, there is no such correlation for the Na-amphiboles (solid circles). The relationship between both *b* and *c* and *A* is similar, displaying a horizontal V-shaped correlation. As seen in Fig. 5, there is an inversion between the PCHvCl amphiboles synthesized in dilute $FeCl_2$ brines and the rest of the PCHvCl amphiboles formed in more concentrated brines. This inversion carries over to Fig. 7, where amphiboles formed in dilute brines have a negative correlation between *A* and both *b* and *c*, while those formed in more concentrated brines have a positive correlation. Beta shows essentially no variation with *A*. Regarding unit cell volume, amphiboles formed in dilute brines show essentially no correlation with *A*, which is the net result of increases in *a* countered by decreases in *b* and *c*, while those formed in concentrated brines show an overall positive correlation with *A*.

Figure 8 shows the relationship between the ^{C}Al and unit cell parameters. Despite the large uncertainties in ^{C}Al content, there is a general contraction of the unit cell as ^{C}Al (0.535 Å) is substituted for $^{C}Fe^{2+}$ (0.78 Å) or $^{C}Fe^{3+}$ (0.645 Å) (Shannon, 1976). The best correlation exists between *b* and ^{C}Al where all amphiboles are essentially colinear.

Figure 9 shows the relationship between the $^{C}Fe^{2+}$ and unit cell parameters for the variable Fe# amphiboles (Fig. 9a) and the Mg-free amphiboles (Fig. 9b). As seen in Fig. 2, there is a great deal of variation in the data among the Mg-free amphiboles, whereas the variable Fe# amphiboles have a strong positive correlation between $^{C}Fe^{2+}$ and *a*, *b*, *c*, and volume.

4 Discussion

4.1 Compositional controls on unit cell parameters

Amphiboles are complex minerals because they have many interrelated chemical substitutions. Consequently, it is difficult to change one chemical variable independently of the others, making the correlation of cell parameters to composition challenging. Therefore, multivariate linear regression was applied to the composition vs. unit cell parameter data for the amphiboles from this study (Table 6). Sta-

tistical p tests were used to determine whether a given element in a specific crystallographic site was correlated with the unit cell parameters ($p < 0.05$). Consideration of the regression coefficients in Table 6 provides insights into how the unit cell parameters are affected by the composition of the amphibole. For example, a negative coefficient for a given parameter suggests a shortening, whereas a positive coefficient suggests a lengthening, and the value of the coefficient is proportional to the magnitude of the effect. These results can be qualitatively compared to the multivariate regression done by Hawthorne and Oberti (2007). Like Hawthorne and Oberti (2007), this study finds the a parameter is very sensitive to the K content and substitution of the C-group cations. Additionally, we find the a parameter is well-correlated with the Cl content of the amphibole, where increasing Cl causes contraction along the a edge. As reported in Hawthorne and Oberti (2007), this study finds the b parameter to be most sensitive to substitutions at the octahedral and the O(3) sites, though Hawthorne and Oberti (2007) did not include Cl in their regression analysis. We also find the b parameter to be strongly correlated with ^{T}Al. The regression indicates that the c parameter responds similarly to changes in composition as the b parameter, being most sensitive to the Cl, $^{C}Fe_{Total}$, and ^{T}Al content. Hawthorne and Oberti (2007) did not find a correlation between the O(3) site and the c parameter, though they did find c to be correlated with the C cations and the ^{T}Al content. Our regression indicates that β is sensitive to substitutions of the C cations, substitutions of the B cations, the K content, and the Cl content, with the latter two having the strongest correlations. In contrast, Hawthorne and Oberti (2007) found the type of B cation and amount of ^{T}Al to be the most important factors affecting β.

The multivariate regression results identified correlations that were not detected when only comparing two variables at a time, such as those between the unit cell parameters and ^{B}Ca and ^{T}Al. The regression results also provide more direct evidence for the correlations observed in Figs. 6–9, such as the correlations between both the b and c parameters and Cl (Fig. 6). It is unlikely that the correlations present between the b and c parameters and Cl are the result of an indirect correlation involving $^{C}Fe_{Total}$ because Cl is always more strongly correlated with the unit cell parameters than the C cations. For example, a linear regression of the PCHvCl amphiboles (Mg-free) between Cl and b has an r^2 value of 0.973, whereas a linear regression between ^{C}Al and b has an r^2 value of 0.713. The multivariate regression analysis yielded similar results; i.e., Cl better correlated with b and c than the C cations (Table S1 in the Supplement).

4.2 The effect of Cl on amphibole structure

Perhaps the most interesting finding here is the effect of Cl on the unit cell parameters. The regression predicts an expansion of 0.181 Å (0.99 %) and 0.048 Å (0.90 %) along the b and c edges respectively, a reduction in β by 0.76° (0.72 %), which makes the unit cell more orthogonal, and a contraction of 0.060 Å (0.59 %) along a when fully substituting Cl for OH in potassic-hastingsite. This contraction along a may seem a bit counterintuitive given the large size of the Cl anion relative to OH but makes more sense through the lens of the mechanism for Cl incorporation given in Oberti et al. (1993). That paper hypothesizes two simultaneously operating mechanisms. The first involves the displacement of Cl away from the O(3) site toward the A cavity; the second is accomplished through the expansion of the octahedral strip along [011], which is suggested here by the expansion of b and c with Cl incorporation. The paper states that as Cl moves toward the A cavity and increasing amounts of Cl are incorporated, bonding should be established and later enhanced between the A cation and Cl. Though the present project lacks the resolution to accurately measure the A–Cl bond length, the contraction along the a edge with increasing Cl can be interpreted as increased bonding between the A-site cation and Cl, which is acting to shorten the unit cell along [100]. The species of A cation should also affect this, depending on its size. Unfortunately, there are not enough data on pure Na chloro-amphiboles to test whether the magnitude of contraction along the a edge is enhanced when the larger K is the A cation relative to Na.

Furthermore, the tetrahedral chains must lengthen to accommodate the expansion of the octahedral strip associated with the substitution of Cl for OH. This can be accomplished by either straightening the tetrahedral chains or substituting ^{T}Al for ^{T}Si, which would enlarge the tetrahedra. Though ^{T}Al has been established here as expanding the amphiboles along the c edge (Table 6), it is not correlated with Cl. Volfinger et al. (1985) suggest that the Cl content of trioctahedral micas and presumably amphiboles should increase with the Si/(Si+^{IV}Al) ratio, where increasing Si content causes chain straightening in monoclinic amphiboles (Hawthorne, 1979). Unfortunately, this project lacks the resolution to measure small changes in the O(5)–O(6)–O(5) angle to characterize the straightness of the tetrahedral chains, and therefore we are not able to confirm this correlation. Although ^{T}Al does not seem to influence Cl incorporation in the amphiboles from this study, many natural amphiboles are reported to have positive correlations between ^{T}Al and Cl, such as the studies of Morrison (1991), Enami et al. (1992), Kullerud (1996), McCormick and McDonald (1999), and Henry and Daigle (2018). This discrepancy is not well understood at present, and it is unclear why natural amphiboles tend toward ^{T}Al enrichment with increasing Cl content.

The findings of this study pose some additional questions for future research.

1. Does $^{T}Fe^{3+}$ occur in Cl-rich amphiboles? Some of the most Cl-rich amphiboles from this study have up to ~ 0.3 apfu $^{T}Fe^{3+}$; due to their deficiency in ^{T}Al, some Fe^{3+} is required to fill the T sites. Tetrahedral Fe^{3+} is not something that is commonly reported in amphi-

Table 6. Regression coefficients obtained by multivariate regression of the composition vs. unit cell parameters for the amphiboles synthesized in this study. This data was also used to calculate the unit cell parameters of ideal potassic-chloro-hastingsite (PCH_i).

Parameter	Ψ_i^a (Å)	Ψ_i^b (Å)	Ψ_i^c (Å)	Ψ_i^β (°)
Intercept	9.5539 (698)	17.8516 (584)	5.2817 (108)	103.7621 (3751)
^{T}Al	−0.0268 (90)	−0.0651 (80)	0.0206 (42)	–
^{C}Fe$_{Total}$	0.0348 (52)	0.0465 (51)	0.0109 (21)	−0.0843 (299)
^{B}Ca	0.1275 (423)	0.1422 (364)	–	0.7375 (2413)
^{A}Na	–	0.0273 (86)	−0.0250 (81)	
^{A}K	0.1681 (100)	–	−0.0285 (80)	0.7623 (563)
Cl	−0.0299 (51)	0.0903 (45)	0.0240 (23)	−0.3790 (294)
	Calculated PCH_i unit cell parameters			
Calculated values	10.038 (10) Å	18.419 (9) Å	5.3970 (4)	104.82 (6) Å

boles, though it has been documented in micas (Miyano and Miyano, 1982; Dyar and Burns, 1986; Cuadros et al., 2019). The substitution of ^{T}Fe^{3+} (0.49 Å) for ^{T}Al^{3+} (0.39 Å) would enlarge the tetrahedral sites and encourage Cl incorporation according to the model of Oberti et al. (1993).

2. How does ^{T}Al affect the Cl content of the amphibole? The source of positive correlations between ^{T}Al and Cl in natural Cl-rich amphiboles is challenged by the findings of this study, which suggests the species of T cation is not that important for incorporating Cl into amphiboles. This question could be addressed if a series of Cl-rich amphiboles differing only in their tetrahedral Al contents could be synthesized. In most cases, however, the tetrahedral Al content is strongly linked with *A*-site occupancy, making it difficult to isolate the role of tetrahedral Al by itself.

4.3 Molar volume of potassic-chloro-hastingsite (PCH_i)

The molar volume of ideal or endmember potassic-chloro-hastingsite (PCH_i), or indeed any chlorine end-member amphibole, is not known at present. However, volume information is necessary for any thermodynamic treatment where variable pressures are involved. Therefore, the molar volume was determined here by using the multivariate regression coefficients for the amphiboles of this study (Table 6). The unit cell parameters of PCH_i were calculated by multiplying the corresponding regression coefficients ($\Psi_i^{a,b,c,\beta}$) by the molar coefficients (n_i) for each component of ideal PCH on the basis of 24 O + OH + Cl. For example, to calculate the a parameter for PCH, we have

$$a\,(\text{Å}) = \Psi_0^a + \left(\Psi_{A_K}^a\right)\left(n_{A_K}\right) + \left(\Psi_{B_{Ca}}^a\right)\left(n_{B_{Ca}}\right) + \left(\Psi_{C_{Fe_{Total}}}^a\right)\left(n_{C_{Fe_{Total}}}\right) + \left(\Psi_{T_{Al}}^a\right)\left(n_{T_{Al}}\right) + \left(\Psi_{O(3)_{Cl}}^a\right)\left(n_{O(3)_{Cl}}\right) = 10.038\,\text{Å}, \quad (1)$$

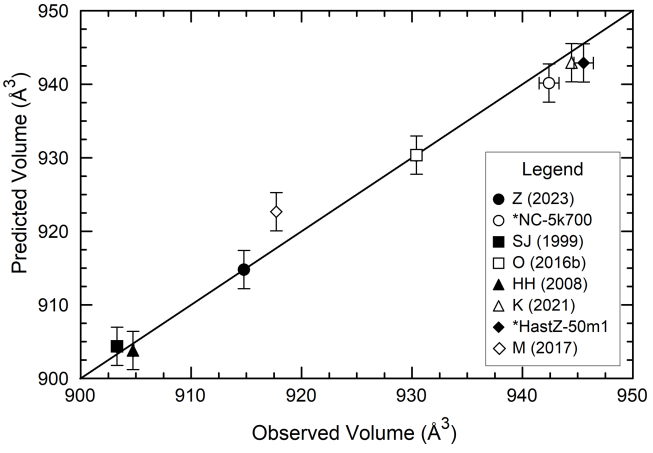

Figure 10. Comparison of unit cell volumes calculated using the multivariate linear regression coefficients of Table 7 and Eq. (1) compared to the observed volumes for a random selection of calcium amphiboles. The diagonal line represents a 1 : 1 correlation. The source study followed by the sample code (if present) is listed in the legend. * indicates an amphibole from this study. Study abbreviations and samples plotted: Z – Zaitsev et al. (2013), OL22; SJ – Sharma and Jenkins (1999), Parg16-6; O – Oberti et al. (2016b), 1260; HH – Hawthorne and Harlow (2008), MS; K – Kaneva et al. (2021); and M – Mueller et al. (2017), hast5-70.

where Ψ_0 is the y intercept of regression. The calculated unit cell parameters are listed in Table 6. The molar volume of PCH_i, calculated according to $V = a, b, c, \sin\beta$, was determined to be 964.63 ± 1.29 Å^3, which is 290.5 ± 0.4 cm^3 mol^{-1} or 29.05 kJ kbar^{-1}.

4.4 Molar volumes of other Cl-amphiboles

Data from this study also provide insight into estimating the unit cell parameters of other end-member Cl-amphiboles. The composition and unit cell data for a combination of amphiboles from this study and several calcium amphiboles reported in other studies (Table S2) were compared with mul-

Table 7. Coefficients for predictive equations for the unit cell parameters obtained by multiple regression of a combination of the amphiboles from this study and those listed in Table S2.

Component	Ψ_i^a (Å)	Ψ_i^b (Å)	Ψ_i^c (Å)	Ψ_i^β (°)
^{T}Al	−0.0322 (75)	−0.0772 (67)	0.0129 (22)	0.1156 (451)
${}^C\mathrm{Fe_{Total}}$	0.0168 (24)	0.0532 (23)	0.0110 (8)	−0.06503 (157)
Mn	–	0.2471 (627)	0.0706 (236)	−1.2068 (4088)
Ti	−0.1583 (322)	–	0.0410 (112)	−0.6606 (1932)
^{B}Ca	–	–	0.0356 (107)	–
${}^B\mathrm{Fe^{2+}}$	−0.0838 (242)	–	0.0388 (128)	−0.5594 (1506)
^{B}Mg	–	–	–	−0.8064 (2952)
^{B}Na	−0.1537 (95)	−0.1912 (94)	0.0451 (112)	−0.6273 (593)
^{A}Na	0.1367 (138)	0.0563 (131)	−0.0169 (34)	0.4714 (851)
^{A}K	0.2719 (168)	0.0908 (145)	–	1.0214 (1027)
F	−0.0197 (64)	−0.0221 (59)	–	–
Cl	−0.0516 (80)	0.0768 (76)	0.0206 (27)	−0.5209 (494)
Ψ_0^i (y intercept)	9.8238 (72)	18.0604 (70)	5.2074 (197)	104.8097 (683)
Adjusted R^2	0.949	0.983	0.963	0.898
Standard error	0.021	0.020	0.0072	0.125

tivariate linear regression. The same methodology was used as described above for PCH_i, and the unit cell parameters of the desired calcium amphibole can be calculated following the outline of Eq. (1). The regression output is listed in Table 7. Figure 10 shows the agreement between the observed and calculated volumes for a random selection of amphiboles from both this study and the literature that were not included in the regressions. This method was also used to estimate the molar volumes of other endmember chloro-amphiboles, as was done for PCH_i, and are listed as follows:

chloro-hastingsite
$(\mathrm{NaCa_2(Fe_4^{2+}Fe^{3+})Al_2Si_6O_{22}Cl_2}) = 947.8 \pm 2.6\,\text{Å}^3$,

chloro-ferropargasite
$(\mathrm{NaCa_2(Fe_4^{2+}Al)Al_2Si_6O_{22}Cl_2}) = 941.2 \pm 2.6\,\text{Å}^3$,

potassic-chloro-ferropargasite
$(\mathrm{KCa_2(Fe_4^{2+}Al)Al_2Si_6O_{22}Cl_2}) = 956.6 \pm 2.6\,\text{Å}^3$, and

chloro-pargasite
$(\mathrm{NaCa_2(Mg_4Al)Al_2Si_6O_{22}Cl_2}) = 915.3 \pm 2.6\,\text{Å}^3$.

5 Conclusions

The composition and unit cell parameters were determined for a group of 25 synthetic hastingsitic amphiboles having a wide range of Cl content (0.00–1.68 apfu). The Cl concentration of the amphibole was determined to increase with pressure over the range explored here (0.3–2.0 GPa). Compositional trends indicate that the substitution of both ${}^C\mathrm{Fe^{2+,3+}}$ for ^{C}Mg and ${}^C\mathrm{Fe^{2+,3+}}$ for ^{C}Al enhance Cl incorporation, with the former having a much larger effect. The A site is positively correlated with Cl in all amphiboles except those synthesized in dilute $\mathrm{FeCl_2}$ brines ($< 6\,m$), which are negatively correlated. This negative trend is attributed to increasing ferric iron replacing both ferrous iron and the A-site cation by the substitution $A^+ + {}^C\mathrm{Fe^{2+}} \leftrightharpoons {}^A\square + {}^C\mathrm{Fe^{3+}}$ occurring during synthesis in increasingly concentrated $\mathrm{FeCl_2}$ brines. It is unclear whether the A-site occupancy directly constrains the Cl content of the amphibole due to the various coupled substitutions that also affect the A-site occupancy, such as the previous reaction or the exchange $A^+ + {}^T\mathrm{Al^{3+}} \leftrightharpoons {}^A\square + {}^T\mathrm{Si^{4+}}$. The results of this study agree with the findings of Matteucci et al. (2024) in that the type of A-site cation (Na vs. K) does not seem to influence the Cl content of the amphibole. No correlations are present between ^{T}Al and Cl. Multivariate linear regression of the composition vs. unit cell dimension data indicates an expansion of 0.181 Å (0.99 %) and 0.048 Å (0.90 %) along the b and c edges respectively, a reduction in β by 0.76° (0.72 %), and a contraction of 0.060 Å (0.59 %) along a when fully substituting Cl for OH in potassic-hastingsite. The multiple linear regression equations allow the prediction of molar volumes for select endmember chloro-amphiboles, such as potassic-chloro-hastingsite $= 964.63 \pm 1.29\,\text{Å}^3$, which is $290.5 \pm 0.4\,\mathrm{cm^3\,mol^{-1}}$ or $29.05\,\mathrm{kJ\,kbar^{-1}}$.

Data availability. All data derived from this research are presented in the enclosed tables and figures in the main text, the Supplement, and Matteucci et al. (2024).

Supplement. The supplement related to this article is available online at: https://doi.org/10.5194/ejm-36-247-2024-supplement.

Author contributions. JPM and DMJ conceptualized the project. JPM performed experiments and did the EMPA and data analysis. MDD carried out the Mössbauer analysis. The manuscript was written by JPM with contributions by DMJ and MDD. Acquisition of the financial support for the project was provided by DMJ.

Competing interests. The contact author has declared that none of the authors has any competing interests.

Disclaimer. Publisher's note: Copernicus Publications remains neutral with regard to jurisdictional claims made in the text, published maps, institutional affiliations, or any other geographical representation in this paper. While Copernicus Publications makes every effort to include appropriate place names, the final responsibility lies with the authors.

Acknowledgements. We are very grateful to David Collins and Jay Thomas for their help with the microprobe analyses at Binghamton University and Syracuse University, respectively. The manuscript benefited greatly from the comments of two anonymous reviewers.

Financial support. This research has been supported by the National Science Foundation (grant no. EAR-1725053).

Review statement. This paper was edited by Stefano Poli and reviewed by two anonymous referees.

References

Angel, R. J.: High-pressure structure of anorthite, Am. Mineral., 73, 1114–1119, 1988.

Barnes, J. D. and Cisneros, M.: Mineralogical control on the chlorine isotope composition of altered oceanic crust, Chem. Geol., 326–327, 51–60, 2012.

Castelli, D.: Chlorpotassium ferro-pargasite from Sesia-Lanzo marbles (Western Italian Alps): a record of highly saline fluids, Soc. Italiana Mineral. Petrol., 43, 129–138, 1988.

Cuadros, J., Michalski, J. R., Dyar, M. D., and Dekov, V.: Controls on tetrahedral Fe(III) abundance in 2:1 phyllosilicates, Am. Mineral., 104, 1608–1619, 2019.

Driscall, J., Jenkins, D. M., Dyar, M. D., and Bozhilov, K. N.: Cation ordering in synthetic low-calcium actinolite, Am. Mineral., 90, 900–911, 2005.

Dyar, M. D. and Burns, R. G.: Mössbauer spectral study of ferruginous one-layer trioctahedral micas, Am. Mineral., 71, 955–965, 1986.

Ekström, T. K.: The distribution of fluorine among some coexisting minerals, Contrib. Mineral. Petrol., 34, 192–200, 1972.

Enami, M., Liou, J. G., and Bird, D. K.: Cl-bearing amphibole in the Salton Sea geothermal system, California, Can. Mineral., 30, 1077–1092, 1992.

Eugster, H. P.: Heterogeneous reactions involving oxidation and reduction at high pressures and temperatures, J. Chem. Phys., 26, 1760–1761, 1957.

Frezzotti, M. L., Ferrando, S., Peccerillo, A., Petrelli, M., Tecce, F., and Perucchi, A.: Chlorine-rich metasomatic H_2O-CO_2 fluids in amphibole-bearing peridotite from Injibara (Lake Tana region, Ethiopian plateau): Nature and evolution of volatiles in the mantle of a region of continental flood basalts, Geochim. Cosmochim. Ac., 74, 3023–3039, 2011.

Frost, B. R.: Introduction to oxygen fugacity and its petrologic importance, in: Oxide minerals: petrologic and magnetic significance, edited by: Lindsley, D. H., Rev. Mineral., De Gruyter, Vol. 25, 1–9, https://doi.org/10.1515/9781501508684, 1991.

Hawthorne, F. C.: The crystal chemistry of the amphiboles. X. Refinement of the crystal structure of ferroglaucophane and an ideal polyhedral model for clinoamphiboles, Can. Mineral., 17, 1–10, 1979.

Hawthorne, F. C. and Harlow, G. E.: The crystal chemistry of Al-rich amphiboles: sadanagaite and potassic-ferrisadanagaite, Can. Mineral., 46, 151–162, 2008.

Hawthorne, F. C. and Oberti, R.: Amphiboles: crystal chemistry, in: Amphiboles: crystal chemistry, occurrence, and health issues, edited by: Hawthorne, F. C., Oberti, R., Della Ventura, G., and Mottana, A., Rev. Mineral. Geochem., De Gruyter, Vol. 67, 1–54, https://doi.org/10.1515/9781501508523-002, 2007.

Henry, D. J. and Daigle, N. M.: Chlorine incorporation into amphibole and biotite in high-grade iron-formations: Interplay between crystallography and metamorphic fluids, Am. Mineral., 103, 55–68, 2018.

Jenkins, D. M.: The incorporation of Cl into calcium amphiboles, Am. Mineral., 104, 514–524, 2019.

Jenkins, D. M., Della Ventura, G., Oberti, R., and Bozhilov, K.: Synthesis and characterization of amphiboles along the tremolite-glaucophane join, Am. Mineral., 98, 588–600, 2013.

Kaneva, E., Radomskaya, T., Shendrik, R., Chubarov, V., and Danilovsky, V.: Potassic-hastingsite from the Kedrovy District (East Siberia, Russia): petrographic description, crystal chemistry, spectroscopy, and thermal behavior, Minerals, 11, 1049, https://doi.org/10.3390/min11101049, 2021.

Kendrick, M. A., Honda, M., and Vanko, D. A.: Halogens and noble gases in Mathematician Ridge meta-gabbros NE Pacific: implications for oceanic hydrothermal root zones and global volatile cycles, Contrib. Mineral. Petrol., 170:43, 2015.

Kullerud, K.: Chlorine-rich amphiboles: interplay between amphibole composition and an evolving fluid, Eur. J. Mineral., 8, 355–370, https://doi.org/10.1127/ejm/8/2/0355, 1996.

Kusebauch, C., John, T., Barnes, J. D., Klügel, A., and Austrheim, H. O.: Halogen element and stable chlorine isotope fractionation caused by fluid-rock interaction (Bamble Sector, SE Norway), J. Petrol., 56, 299–324, 2015.

Léger, A., Rebbert, C., and Webster, J.: Cl-rich biotite and amphibole from Black Rock Forest, Cornwall, New York, Am. Mineral., 81, 495–504, 1996.

Levien, L., Prewitt, C. T., and Weidner, D. J.: Structure and elastic properties of quartz at pressure, Am. Mineral., 65, 920–930, 1980.

Liu, J., Liu, W., Ye, K., and Mao, Q.: Chlorine-rich amphibole in Yangkou eclogite, Sulu ultrahigh-pressure meta-

morphic terrane, China, Eur. J. Mineral., 21, 1265–1285, https://doi.org/10.1127/0935-1221/2009/0021-1968, 2009.

Makino, K., Tomita, K., and Suwa, K.: Effect of chlorine on the crystal structure of a chlorine-rich hastingsite, Mineral. Mag., 57, 677–685, 1993.

Matteucci, J. P., Jenkins, D. M., and Dyar, M. D.: The effect of the ^{A}Na-^{A}K ratio on chlorine incorporation into hastingsitic amphiboles, Am. Mineral., in review, 2024.

McCormick, K. A. and McDonald, A. M.: Chlorine-bearing amphiboles from the Fraser Mine, Sudbury, Ontario, Cananda: description and crystal chemistry, Can. Mineral., 37, 1385–1403, 1999.

Miyano, T. and Miyano, S.: Ferri-annite from the Dales Gorge Member iron-formations, Wittenoom area, Western Australia, Am. Mineral., 67, 1179–1194, 1982.

Morosin, B. and Graeber, E. J.: Crystal structures of manganese (II) and iron (II) chloride dihydrate, J. Chem. Phys., 42, 898–901, 1965.

Morrison, J.: Compositional constraints on the incorporation of Cl into amphiboles, Am. Mineral., 76, 1920–1930, 1991.

Mueller, B. L., Jenkins, D. M., and Dyar, D. M.: Chlorine incorporation in amphiboles synthesized along the magnesio-hastingsite–hastingsite compositional join, Eur. J. Mineral., 29, 167–180, https://doi.org/10.1127/ejm/2017/0029-2606, 2017.

Newton, R. C., Aranovich, L. Y., Hansen, E. C., and Vandenhuevel, B. A.: Hypersaline fluids in Precambrian deep-crustal metamorphism, Precamb. Res., 91, 41–63, 1998.

Novak, G. A. and Gibbs, G. V.: The crystal chemistry of silicate garnets, Am. Mineral., 56, 791–825, 1971.

Oberti, R., Ungaretti, L., Cannillo, E., and Hawthorne, F. C.: The mechanism of Cl incorporation in amphibole, Am. Mineral., 78, 746–752, 1993.

Oberti, R., Boiocchi, M., Hawthorne, F. C., Ball, N. A., Cámara, F., Pagano, R., and Pagano, A.: Ferro-ferri-hornblende from the Traversella mine (Ivrea, Italy): occurrence, mineral description, and crystal-chemistry, Mineral. Mag., 80, 1233–1242, 2016b.

Oberti, R., Boiocchi, M., Zema, M., Hawthorne, F. C., Redhammer, G. J., Susta, U., and Della Ventura, G.: The high-temperature behavior of riebeckite: expansivity, deprotonation, selective Fe oxidation and a novel cation disordering scheme for amphiboles, Eur. J. Mineral., 30, 437–449, https://doi.org/10.1127/ejm/2018/0030-2712, 2018.

Ohashi, Y. and Finger, L. W.: Refinement of the crystal structure of sanidine at 25 and 400 °C, Carnegie I. Wash., 73, 539–544, 1974.

Quirion, D. and Jenkins, D.: Dehydration and partial melting of tremolitic amphibole coexisting with zoisite, quartz, anorthite, diopside, and water in the system H_2O-CaO-MgO-Al_2O_3-SiO_2, Contrib. Mineral. Petr., 130, 379–389, 1998.

Redhammer, G. J., Beran, A., Schneider, J., Amthauer, B., and Lottermoser, W.: Spectroscopic and structural properties of synthetic micas on the annite-siderophyllite binary: Synthesis, crystal structure refinement, Mössbauer, and infrared spectroscopy, Am. Mineral., 85, 449–465, 2000.

Sautter, V., Jambon, A., and Boudouma, O.: Cl-amphibole in the nakhlite MIL 03346: Evidence for sediment contamination in a Martian meteorite, Earth Planet. Sc. Lett., 252, 45–55, 2006.

Selverstone, J. and Sharp, Z. D.: Chlorine isotope evidence for multicomponent mantle metasomatism in the Ivrea Zone, Earth Planet. Sc. Lett., 310, 429–440, 2011.

Schneider, J. B. and Jenkins, D. M.: Stability of sodalite relative to nepheline and NaCl-H_2O brines at 750 °C: Implications for hydrothermal formation of sodalite, Can. Mineral., 58, 3–18, 2020.

Shannon, R.: Revised effective ionic radii and systematic studies of interatomic distances in halides and chalcogenides, Acta Crystallogr. A, 32, 751–767, 1976.

Sharma, A. and Jenkins, D. M.: Hydrothermal synthesis of amphiboles along the tremolite-pargasite join and in the ternary system tremolite-pargasite-cummingtonite, Am. Mineral., 84, 1304–1318, 1999.

Smyth, J. R. and Hazen, R. M.: The crystal structure of forsterite and hortonolite at several temperatures, Am. Mineral., 58, 588–593, 1973.

Taylor, J. R., Wall, V. J., and Pownceby, M. I.: The calibration and application of accurate redox sensors, Am. Mineral., 77, 284–295, 1992.

Toby, B. H. and Von Dreele, R. B.: GSAS-II: The genesis of a modern open-source all purpose crystallography software package, J. Appl. Crystallogr., 46, 544–549, 2013.

Volfinger, M., Robert, J. L., Vielzeuf, D., and Neiva, M. R.: Structural control of the chlorine content of OH-bearing silicates (micas and amphiboles), Geochim. Cosmochim. Ac., 49, 37–48, 1985.

Walker, D., Cranswick, L. D., Jones, R. L., Clark, S. M., and Buhre, S.: Halite-sylvite thermoelasticity, Am. Mineral., 89, 204–210, 2004.

Waychunas, G. A.: Crystal chemistry of oxides and oxyhydroxides, in: Oxide minerals: petrologic and magnetic significance, edited by: Lindsley, D. H., Rev. Mineral., De Gruyter, Vol. 25, 11–68, https://doi.org/10.1515/9781501508684, 1991.

Wechsler, B. A., Lindsley, D. H., and Prewitt, C. T.: Crystal structure and carbon distribution in titanomagnetites, Am. Mineral., 69, 754–770, 1984.

Weidner, J. R.: Welding silver and silver alloy containers for high-temperature and high-pressure experiments, Am. Mineral., 74, 1385, 1989.

Xiao, Y., Hoefs, J., and Andreas, K.: Compositionally zoned Cl-rich amphiboles from North Dabie Shan, China: Monitor of high-pressure metamorphic fluid/rock interaction processes, Lithos, 81, 279–295, 2005.

Yardley, B. and Bodnar, R. I.: Fluids in the Continental Crust, Geochem. Perspect., 3, 1–127, 2014.

Yu, M., Feng, C. Y., Zhu, Y. F., Mao, J. W., Zhao, Y. M., and Li, D. X.: Multistage amphiboles from the Galinge skarn deposit in Qiman Tagh, western China: evidence of igneous rocks replacement, Mineral. Petrol., 111, 81–97, 2017.

Zaitsev, A. N., Avdontseva, E. Y., Britvin, S. N., Dèmeny, A., Homonnay, Z., Jeffries, T. E., Keller, J., Krivovichev, V. G., Markl, G., Platonova, N. V., Siidra, O. I., Spratt, J., and Vennemann, T.: Oxo-magnesio-hastingsite, $NaCa_2(Mg_2Fe^{3+}_3)(Al_2Si_6)O_{22}O_2$, a new anhydrous amphibole from the Deeti volcanic cone, Gregory rift, northern Tanzania, Mineral. Mag., 77, 2773–2792, 2013.

Zhang, L., Ahsbahs, H., Hafner, S. S., and Kutoglu, A.: Single-crystal compression and crystal structure of clinopyroxene up to 10 GPa, Am. Mineral., 82, 245–258, 1997.